

**SYNTHESIS AND CHARACTERIZATION OF MUNICIPAL WASTE  
INCINERATOR FLY ASH BASED GEOPOLYMERS FOR THE REMOVAL OF  
ENDOSULFAN FROM WATER: KINETICS, ISOTHERMS, AND  
THERMODYNAMICS**

**BY  
ISAAC LUTTAH**

**A THESIS SUBMITTED IN PARTIAL FULFILMENT OF THE REQUIREMENTS  
FOR THE DEGREE OF MASTER OF SCIENCE IN CHEMISTRY**

**SCHOOL OF PHYSICAL AND BIOLOGICAL SCIENCES**

**MASENO UNIVERSITY**

**© 2024**

## DECLARATION

I certify that this thesis is my original work and has not been previously presented for a degree award in Maseno University or any other university. All sources of information have been supported by relevant references.

**Mr Isaac Luttah,**  
**MSC/SC/00020/2018**

Signature: ..... Date: 27/11/2023 .....

### Supervisors

This thesis has been submitted for examination upon the approval of:

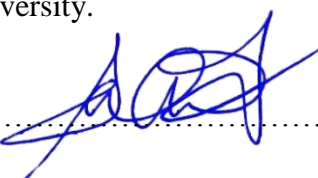
**1) Prof. Chrispin Kowenje,**

Assoc. Prof. at Department of Chemistry,  
School of Physical and Biological Sciences,  
Maseno University.

Signature:  ..... Date: 27/11/2023 .....

**2) Dr. Daniel Onunga,**

Lecturer at Department of Chemistry,  
School of Physical and Biological Sciences,  
Maseno University.

Signature:  ..... Date: 27/11/2023 .....

**3) Dr. Victor Shikuku,**

Lecturer at Department of Physical Sciences,  
Kaimosi Friends University.

Signature:  ..... Date: 27/11/2023 .....

## **ACKNOWLEDGEMENT**

First and foremost, my appreciation goes to my first supervisor and lecturer, Prof. Chrispin O. Kowenje for his guidance, motivation and positive criticism in every step of this study. I am grateful to Dr. Victor O. Shikuku of Kaimosi Friends University for his enormous contribution and support right from conceptualisation of this research work and resource mobilisation. My appreciation also goes to Dr. Daniel Onunga of Maseno University for his guidance and supervision.

I would like to thank Dr. Benton Onyango Otieno of Vaal University of Technology-South Africa, Dr. Daniel Onunga of Maseno University, and Dr. Pierre Kalenga Mubiayi (University of the Witwatersrand, Johannesburg) for their support in facilitating the experimental aspects of this thesis work.

I thank chemistry department, Maseno University for providing support for this research work. I express my gratitude to Kaimosi Friends University for partly funding this project through Kaimosi Friends University Internal Research Grant (KAF/601/APPL/043/1(6)).

I give special appreciation to my family for their encouragement and prayers throughout the course of my studies.

Finally, I thank the Almighty God for His favour and provision throughout the period of my studies.

## **DEDICATION**

To my parents, 'Repher Achayo Amuyeka and Joseph Amuyeka Odongo'.

Thank you.

## ABSTRACT

Endosulfan is a broad spectrum organochlorine insecticide which acts as a contact poison for controlling a wide variety of insects. However, extensive and uncontrolled use of insecticides leads to water pollution. Conventionally, adsorption onto activated carbon is used to remove water pollutants from influent wastewater. A suitable adsorbent must be cheap, possess high adsorption capacity, fast adsorption kinetics and recyclable among other properties. Geopolymers are emerging low-cost and efficient adsorbents for removal of various contaminants from water. The performance of the geopolymers varies with both sorption conditions and adsorbent structural and textural characteristics, which are controlled by several factors such as; the precursor material and the preparation conditions. While silicate to NaOH ratios affect mechanical properties of geopolymers for construction purposes, the impact of silicate to NaOH ratios on the adsorptive performance of geopolymers is unknown. Furthermore, although research has been done on remediation of pesticides from water using various adsorbents, no article has reported the use of solid waste incinerator fly ash MWFA-based geopolymers especially on their synthesis and/or application as adsorbent for endosulfan removal from water. The present work investigated the adsorption of endosulfan on alkaline activated geopolymers, synthesized from MWFA. Since there is no reported theory for predicting the geopolymer sorption capacity and adsorption rate based on precursor materials and silicate to NaOH ratios conditions, this leaves a clear gap in our understanding of the role of these factors. The objective of this study was to synthesize MWFA-based geopolymers and evaluate the effect of sodium silicate to NaOH ratio of the activator solution on morphology, chemical composition, and adsorptive performance (adsorption capacity and mechanism) in batch-mode. Alkali-activated MWFA-based geopolymers, GPA, GPB, and GPC, were synthesized using 0.17, 0.21 and 0.24 sodium silicate to sodium hydroxide mole ratios, respectively. The geopolymers were applied in the removal of endosulfan from water. The adsorbents were characterized by XRD, SEM-EDX, and FTIR. Variation of sodium silicate to sodium hydroxide mole ratios resulted in morphologically distinguishable geopolymers with different compositions. Adsorption experiments were done at different parameters such as initial endosulfan concentration, contact time, pH, geopolymer dosage and temperature. The adsorption equilibrium data were best described by Langmuir isotherm. The maximum adsorption capacities increased with an increase in sodium silicate to sodium hydroxide mole ratios in the order 1.872, 15.899, 16.970, and 20.010 mg/g for MWFA, GPA, GPB, and GPC, respectively. The kinetic data were best described by the *pseudo*-first-order model wherein the adsorption rate ( $k_1$ ) was independent of the sodium silicate to sodium hydroxide mole ratio and the geopolymer composition. The thermodynamic parameters, that is enthalpy ( $\Delta H > 0$ ), Gibbs free energy ( $\Delta G < 0$ ), entropy ( $\Delta S > 0$ ), and activation energy ( $E_a > 0$ ) show that the processes were endothermic, spontaneous, physical ( $E_a$  and  $\Delta H < 40$  kJ/mol) and entropy-driven. Alkalinization was beneficial since the geopolymers had a higher adsorption capacity (~8-10 times) and affinity for endosulfan (~30 times) than the precursor material (MWFA). The adsorption mechanism entailed electrostatic interactions and hydrogen bonding. Increase in sodium silicate to NaOH ratio increases the adsorption capacity of the geopolymers for endosulfan. The MWFA-based geopolymers prepared with high silicate to NaOH ratios are recommended as alternative high adsorbing materials for wastewater treatment and a strategy for the valorization of MWFA.

## TABLE OF CONTENT

DECLARATION .....	ii
ACKNOWLEDGEMENT .....	iii
DEDICATION .....	iv
ABSTRACT.....	v
TABLE OF CONTENT .....	vi
LIST OF ABBREVIATIONS AND ACRONYMS .....	viii
LIST OF TABLES .....	ix
LIST OF FIGURES .....	x
LIST OF APPENDICES .....	xi
<b>CHAPTER ONE: INTRODUCTION.....</b>	<b>1</b>
1.1 Background to the Study.....	1
1.2 Statement of the Problem.....	3
1.3 Objectives of the Study .....	4
1.3.1 General Objectives.....	4
1.3.2 Specific Objectives .....	4
1.4 Null Hypotheses.....	4
1.5 Justification of the Study .....	5
1.6 Significance of the Study .....	6
<b>CHAPTER TWO: LITERATURE REVIEW.....</b>	<b>7</b>
2.1 Chemical Nature of Endosulfan.....	7
2.2 Endosulfan Toxicity.....	8
2.3 Endosulfan and Its Application.....	9
2.4 Environmental Fate of Endosulfan .....	9
2.5 Remediation of Endosulfan from Contaminated Water.....	10
2.6 Geopolymers .....	11
2.6.1 Mechanisms of Geopolymer Formation .....	12
2.6.2 Fly ash.....	13
2.6.3 Fly Ash-Based Geopolymers .....	13
<b>CHAPTER THREE: MATERIALS AND METHODS .....</b>	<b>17</b>
3.1 Materials and Chemicals.....	17
3.2 Methodology .....	17

3.2.1 Synthesis of the Geopolymer Adsorbents.....	17
3.2.2 Characterization of the Geopolymer Adsorbents.....	18
3.2.3 Adsorption Experiments .....	18
3.2.4 Adsorption Kinetics .....	20
3.2.5 Thermodynamic Parameters of Adsorption Process.....	21
3.2.6 Adsorption Isotherm Modelling.....	23
3.2.6.1 Langmuir Isotherm Model .....	23
3.2.6.2 Freundlich Isotherm Model.....	24
3.2.7 Statistical Analysis.....	24
<b>CHAPTER FOUR: RESULTS AND DISCUSSION .....</b>	<b>25</b>
4.1 Production of the Geopolymers .....	25
4.2 Characterization Studies of the MWFA and MWFA-based Geopolymers .....	26
4.2.1 Functional Group Identification.....	26
4.2.2 Morphological and Composition Analysis .....	27
4.2.3 Crystallinity and Mineralogical Studies.....	30
4.2.4 Point of Zero Charge (pHpzc) Studies.....	34
4.3 Adsorption Experiments .....	36
4.3.1 Calibration Curves .....	36
4.3.2 Effect of pH on Adsorption Mechanism.....	36
4.3.3 Effect of Initial Concentration .....	38
4.3.4 Effect of Contact Time.....	38
4.3.5 Kinetics Studies .....	39
4.3.6 Thermodynamics of Endosulfan Adsorption .....	41
<b>CHAPTER FIVE: CONCLUSIONS, RECOMMENDATIONS AND SUGGESTIONS FOR FURTHER RESEARCH .....</b>	<b>49</b>
5.1 Conclusions.....	49
5.2 Recommendations.....	50
5.3 Suggestions for Further Research .....	50
<b>REFERENCES.....</b>	<b>51</b>
<b>APPENDICES .....</b>	<b>63</b>

## LIST OF ABBREVIATIONS AND ACRONYMS

<b>DOC</b>	:	Degree of crystallinity
<b>EDX</b>	:	Energy-dispersive X-ray spectroscopy
<b>FOR</b>	:	Free oxygen radicals
<b>FTIR</b>	:	Fourier Transform Infra-Red
<b>GABA</b>	:	Gamma amino butyric acid
<b>GPA</b>	:	Geopolymer A
<b>GPB</b>	:	Geopolymer B
<b>GPC</b>	:	Geopolymer C
<b>Mm</b>	:	Micrometre
<b>MWFA</b>	:	Municipal waste fly ash
<b>OS</b>	:	Oxidative stress
<b>PDF</b>	:	Powder Diffraction File
<b>Ph</b>	:	Negative Logarithm of the Hydrogen Ion Concentration
<b>pH<sub>pzc</sub></b>	:	pH point of zero charge
<b>rpm</b>	:	Rotations per minute
<b>SEM</b>	:	Scanning Electron Microscopy
<b>XRD</b>	:	X-Ray Diffraction



## LIST OF TABLES

Table 3.1: Interpretation of Langmuir separation constant, $R_L$ .....	24
Table 4.1: Elemental composition of precursor (MWFA).....	28
Table 4.2: Elemental composition of MWFA-based geopolymers .....	29
Table 4.3: Variation of adsorption capacity, at, (mg/g) with time (minutes) ( $C_o = 8$ mg/L, $T = 303$ K).....	39
Table 4.4: Lagergren pseudo-first-order (PFO) and Pseudo-second-order (PSO) parameters	40
Table 4-5: Thermodynamic parameters of GPA, GPB, GPC, and MWFA.....	43
Table 4.6: Langmuir and Freundlich isotherm models parameters .....	46
Table 4.7: A comparison of adsorption capacities of MWFA-based geopolymers with other adsorbents for endosulfan .....	48

## LIST OF FIGURES

Figure 2.1: Molecular structure of endosulfan.....	7
Figure 2.2: Schematic pathway for endosulfan degradation.....	10
Figure 2.3: A schematic representation of geopolymer structure .....	12
Figure 2.4: Geopolymerization mechanism.....	13
Figure 4.1: Photographs of MWFA, GPA, GPB, and GPC (Scale - 3:4).....	25
Figure 4.2: FTIR spectrum of MWFA.....	26
Figure 4.3: FTIR spectra of MWFA, GPA, GPB, and GPC.....	26
Figure 4.4: SEM image of MWFA (X230).....	28
Figure 4.5: SEM images of MWFA, GPA, GPB, and GPC at X230 magnification .....	29
Figure 4.6: XRD diffractograms for MWFA.....	30
Figure 4.7: XRD diffractograms for MWFA, GPA, GPB, and GPC.....	33
Figure 4.8: The pH point of zero charge of MWFA.....	35
Figure 4.9: The pH point of zero charge of MWFA, GPA, GPB, and GPC.....	35
Figure 4.10: Calibration curve for endosulfan.....	36
Figure 4.11: Surface charge of the MWFA-based geopolymer in acidic medium .....	37
Figure 4.12: Graph of adsorption capacity and removal efficiency against pH .....	37
Figure 4.13: Variation of adsorption capacity and removal efficiency with initial concentration .....	38
Figure 4-14: Evolution of sorption capacity of GPA, GPB, GPC, and MWFA for endosulfan with time ( $m = 0.1\text{g}/50\text{mL}$ , $C_i = 8\text{mg/L}$ , $\text{pH} = 5$ ) .....	39
Figure 4.15: The Van't Hoff plots for MWFA, GPA, GPB and GPC .....	42
Figure 4.16: Arrhenius-type equation plots for MWFA, GPA, GPB and GPC.....	44

## LIST OF APPENDICES

Appendix 1: Statistical analysis of the kinetic data using originPro 9.0 software.....	63
Appendix 2: Statistical analysis of the thermodynamic data using originPro 9.0 software ....	64
Appendix 3: Statistical analysis of the Langmuir adsorption isotherm data using originPro 9.0 software.....	65
Appendix 4: Langmuir adsorption isotherm using excel.....	66
Appendix 5: Freundlich adsorption isotherm using excel .....	67

# CHAPTER ONE

## INTRODUCTION

### 1.1 Background to the Study

Insecticides are pesticides formulated to kill, harm, repel, or mitigate effects of one or more species of insects through different mechanisms such as disrupting the nervous system, damaging their exoskeletons, repelling them, or controlling them by interfering with their genetics and reproduction (Kegley *et al.*, 2010). Insecticides include ovicides and larvicides applied against target insect eggs and larvae. The application of insecticides in plantations leads to increased yields (Kughur, 2012). However, extensive and uncontrolled use of such agrochemicals may lead to water pollution (Al-Samarai *et al.*, 2018).

Endosulfan (6,9-Methanol-2,4,3-benzodioxathiepin-6,7,8,9,10,10-hexachloro-1,5,5a,6,9,9a-hexahydro-3,3-dioxide) is an organochlorine broad-spectrum insecticide of the cyclodiene subgroup which acts as a contact poison in a wide variety of insects. Most organochlorides act on neurons by causing a sodium/potassium imbalance preventing normal transmission of nerve impulses. Some act on the gamma-aminobutyric acid (GABA) receptor preventing chloride ions from entering the neurons causing a hyperexcitable state characterized by tremors and convulsions. Endosulfan, for example, is a GABA-gated chloride channel antagonist (Sipes *et al.*, 2013). Endosulfan and most other broad-spectrum insecticides have been taken out of use because of their toxicity (Lubick, 2010). However reports show that the pesticide still finds its way into the market and eventually the farmlands (Dewan *et al.*, 2004). Like most agrochemicals, endosulfan gets into water sources through leaching, discharge of untreated industrial effluents, unchecked dumping of used endosulfan containers, farmyard deposition, and surface run-off (Hwang *et al.*, 2018).

Endosulfan is known to cause teratogenic malformations in fish and amphibians and disrupts hormones in frogs, ecological disturbance in freshwater ecosystems through alteration in the composition of planktonic algae species and death of aquatic life, such as shellfish (Lubick, 2010; Patocka *et al.*, 2016). According to Roberts *et al.* (2007), maternal exposure to endosulfan during the first and second trimesters can lead to autism disorders. Considering its toxicity, the environmental fate of endosulfan is of great concern requiring removal from the contaminated sites.

Conventionally, the activated carbon method has been used to remove the pesticide from contaminated water. For example, carbon slurry as a novel adsorbent material for the removal

of endosulfan from contaminated water has been reported (Gupta and Imran, 2008; Kakoi *et al.*, 2015). Elsewhere, Hengpraprom *et al.* (2006) and Polati *et al.* (2006) reported the adsorption of  $\alpha$ -endosulfan onto kaolinite particles and to a mixture of kaolinite and montmorillonite particles from aqueous suspension, respectively.

Similarly, studies on endosulfan adsorption onto hydrophobic zeolites (Yonli *et al.*, 2012) and high silica zeolites (Jiang *et al.*, 2018) have been documented. These studies provide evidence of the suitability of aluminosilicate-based materials as adsorbents for endosulfan removal. Geopolymers are an emerging class of aluminosilicate materials. Recently, it has been shown that geopolymers are emerging low-cost and efficient aluminosilicate adsorbents for the removal of various contaminants such as heavy metals and dyes from water owing to a plethora of precursor materials available for geopolymer development (Shikuku and Sylvain, 2019). The materials evaluated for geopolymer development for water purification include metakaolin (Shikuku *et al.*, 2022), volcanic ash (Tome *et al.*, 2021), pozzolan and biochars composites (Dzoujo *et al.*, 2022), municipal waste incinerator fly ash, MWFA, (Al-Ghout *et al.*, 2020) among others. For example, Craig *et al.* (2015) reported the application of biochar/geopolymer composites in the remediation of pesticides (such as atrazine, dieldrin, picloram, metalochlor, tebuthiuron and hexazinone) from contaminated water. Albeit little research work has been done on the interactions of geopolymers with pesticides in water, no research work has reported the suitability of municipal waste incinerator-fly ash (MWFA)-based geopolymers as adsorbents for endosulfan removal from contaminated water. MWFA-based geopolymers are of great interest in the remediation of insecticides due to the dual advantage of valorization of waste materials and water treatment with the possibility of using the spent geopolymers for construction purposes (Tome *et al.*, 2018).

During geopolymer formation, an aluminosilicate source with sufficient aluminium and silicon percentage composition is reacted with an alkaline activator solution (Siyal *et al.*, 2018). The type of aluminosilicate source, the concentration and type of alkaline activator solution, and the curing temperature affect the properties of the geopolymer formed though the extent is determined by the precursor materials (Tome *et al.*, 2021; Tome *et al.*, 2018). While silicate to NaOH ratios affect the mechanical strength of geopolymers (Abdullah *et al.*, 2011), the effect of silicate to sodium hydroxide mole ratio on the adsorptive properties of geopolymers is unknown for optimization of synthesis conditions for water treatment. Since there is no scientific theory for predicting the geopolymer sorption capacity and adsorption rate based on precursor materials and silicate to NaOH ratios conditions, this leaves a clear

gap in our understanding of the role of these factors. The disposal of MWFA is an unresolved environmental problem that causes secondary pollution. Since MWFA is reported to have sufficient aluminium and silicon content, it can be applied as an aluminosilicate precursor during geopolymer formation (Fabricius *et al.*, 2020). Al-Ghouti *et al.* (2020) reported the use of MWFA-based geopolymer for the removal of dyes from water. However, the effect of synthesis conditions for optimization of the adsorption properties of MWFA-based geopolymers has not been reported as well. A suitable adsorbent must be cheap, possess high adsorption capacity, fast adsorption kinetics and recyclable among other properties. The adsorption rates, capacity and thermodynamic feasibility of adsorption of endosulfan by MWFA-based geopolymers needs to be understood. In this study, the precursor material (MWFA) was reacted with alkaline activator solutions of varied sodium silicate to sodium hydroxide mole ratios to obtain various morphologically different MWFA-based geopolymers. The effect of the sodium silicate to sodium hydroxide mole ratio on the adsorption properties of the MWFA-based geopolymers was investigated, with endosulfan introduced in water as a model pesticide, and is herein reported for the first time.

## **1.2 Statement of the Problem**

Excessive endosulfan application in crop plantations leads to increased contamination of water resources. Human beings, especially farm workers, and other aquatic and terrestrial life consequently become exposed to endosulfan posing a health hazard depending on the residual levels and time of exposure. A number of adsorbents such as activated carbon, industrial fly ash geopolymers, biochars, chitosan, activated alumina, molecular sieve carbon, clays and zeolites are currently applied on different adsorbate during water treatment. Large-scale water treatment facilities require adsorbents that are stable, effective, environmentally friendly, low-cost and sustainably synthesized and regenerated. All the aforementioned adsorbents suffer diverse inherent drawbacks and are locally unavailable in western Kenya counties. There is, therefore, an urgent need to develop effective, low-cost and locally available endosulfan removal techniques to minimize the risk of endosulfan poisoning through water contamination. Geopolymers are effective adsorbents for various water pollutants such as herbicides and dyes. Municipal waste incinerator fly ash (MWFA) has been found to be a suitable precursor for geopolymerization under alkaline activator solution. MWFA is usually disposed of in landfills, pits and open fields which poses secondary environmental pollution. Utilising the MWFA for geopolymer synthesis solves the environmental nuisance and takes the advantage that fly ash is cheap and locally available in

western Kenya counties. The properties, composition and structure of geopolymers depend on the synthesis conditions. However, no reported study precisely evaluates the effect of sodium silicate to sodium hydroxide mole ratio in the alkaline activator on the structural properties and adsorptive performance of MWFA-based geopolymers as a criterion for predicting optimum endosulfan adsorption. An in-depth analysis of effects of initial endosulfan concentration, contact time, pH and temperature on the adsorption of endosulfan on such a specially synthesized MWFA-based geopolymer has not been reported. To understand their interactions fully, the kinetics and thermodynamics for adsorption of endosulfan on MWFA-based geopolymer needs investigation.

### **1.3 Objectives of the Study**

#### **1.3.1 General Objectives**

To evaluate the potential of geopolymer developed from MWFA as an adsorbent for the removal of endosulfan from water.

#### **1.3.2 Specific Objectives**

- i. To determine the optimum sodium silicate to sodium hydroxide mole ratios for MWFA- based geopolymer synthesis.
- ii. To characterize MWFA-based geopolymers synthesized at different sodium silicate to sodium hydroxide mole ratios in alkaline activator solution.
- iii. To determine specific kinetic parameters e.g., contact time, pH, temperature and adsorbent dosage, of endosulfan adsorption on the MWFA-based geopolymer.
- iv. To determine the suitable adsorption isotherm model for adsorption of endosulfan on the MWFA-based geopolymer.

### **1.4 Null Hypotheses**

- i) There is no geopolymerization when MWFA is mixed with an alkaline solution containing sodium silicate and sodium hydroxide mixture.
- ii) There is no change in geopolymer morphological properties and chemical composition as a result of variation in sodium silicate/sodium hydroxide mole ratios in alkaline activator.
- iii) There is no difference in adsorption kinetics and thermodynamics of endosulfan adsorption on the geopolymers synthesized at different sodium silicate/sodium hydroxide mole ratios.

iv) Langmuir and Freundlich adsorption isotherm models are not suitable for describing the adsorption data.

### **1.5 Justification of the Study**

Endosulfan, like most insecticides, has been reported to be a potential toxin that can lead to many human health problems. Being a multi-system poison, endosulfan is capable of causing toxicity to the lungs, kidneys, liver, nerves, heart and muscles. Endosulfan finds its way into the water resources from anthropogenic sources. Its removal from water is therefore important. A number of adsorbents such as activated carbon, industrial fly ash geopolymers, biochars, chitosan, activated alumina, molecular sieve carbon, clays and zeolites are currently applied for the removal of different pollutants during water treatment. Large-scale wastewater treatment requires effective, environmentally friendly, low-cost and locally available (western Kenya counties) adsorbent materials. Currently, activated charcoal is the most effective adsorbent. However, activated charcoal is expensive, not environmentally friendly and recycling process is costly. Therefore, an efficient water treatment technique for contaminant remediation and effective low-cost integrated operations needs to be established. Geopolymers are an emerging class of aluminosilicate adsorbents. Geopolymers are effective adsorbents for various water pollutants such as herbicides and dyes and municipal solid waste fly ash (MWFA) has been found to be a potential precursor for geopolymerization under alkaline activator solution. Municipal waste incinerator fly ash causes environmental pollution since it is usually deposited in landfills, pits and open fields. This study is justified because, utilising the MWFA for geopolymer synthesis solves the environmental nuisance and takes the advantage that fly ash is cheap and locally available. However, the synthesis conditions for maximization of adsorption capacity of MWFA geopolymers is undocumented and needs to be determined.

This study sought to determine the best sodium silicate to sodium hydroxide mole ratio, an important parameter in geopolymer structure, composition and properties, in the alkaline activator resulting in a geopolymer with higher endosulfan adsorption capacity, when parameters such as effects of initial endosulfan concentration, mass of geopolymer, contact time, pH and temperature are considered. An investigation on the effectiveness of adsorption of endosulfan on MWFA-based geopolymer, through kinetics, thermodynamic studies and isotherm models will support the application of MWFA based geopolymers for endosulfan remediation in water treatment systems, and was therefore justified.



The outcome of this study was an understanding of the role of silicate to NaOH ratio on the morphological, compositional and adsorptive properties of MWFA-based geopolymers for endosulfan adsorption. The kinetics and thermodynamic data reported in this study are important for setting standard for MWFA-based geopolymers. The outcomes of this study are MWFA-based geopolymers that are optimum for endosulfan removal in large-scale water treatment systems.

### **1.6 Significance of the Study**

This study contributes to science by providing important kinetic and thermodynamic data is necessary for setting standards of MWFA-based polymers. The Optimal MWFA-based polymers developed in this study are suitable for endosulfan remediation from large scale water treatment systems.

## CHAPTER TWO

### LITERATURE REVIEW

This section discusses chemical nature of endosulfan, endosulfan toxicity, application, environmental fate and remediation of endosulfan from contaminated water. Geopolymers, reaction mechanism of geopolymer formation, fly ash and MWFA are also discussed. Towards the end, kinetics and thermodynamic studies are discussed with reference to previous studies.

#### 2.1 Chemical Nature of Endosulfan

Endosulfan (6,7,8,9,10,10-hexachloro-1,5,5a,6,9,9a-hexahydro-6,9-methanol-2,4,3-benzodioxathiepine-3-oxide) is a cyclic sulphite ester that is 1,5,5a,6,9,9a-hexahydro-6,9-methano-2,4,3-benzodioxathiepine 3-oxide substituted by chloro groups positions 6,7,8,9,10 and 10. It is a broad spectrum organochlorine insecticide of the cyclodiene subgroup which acts as a contact poison in a wide variety of insects and mites. The insecticide was first registered for commercial use in 1954. It is primarily applied on food crops such as tea, fruits, vegetables, grains as well as wood preservation (Jia *et al.*, 2009). Thiodan®, which is the trade name for endosulfan (1,2,3,4,7,7-hexachlorobicyclo-2,2,1-heptene-2,3-bishydroxy methane-5,6-sulfite), is a mixture of two stereoisomers having 70% endosulfan- $\alpha$  (endosulfan I) and 30% endosulfan- $\beta$  (endosulfan II) (Kucuker *et al.*, 2009). Endosulfan sulphate is a product of oxidation containing one extra O atom attached to the S atom (Figure 2.1). The oxidation process imparts the endosulfan with insecticidal properties leading to its extensive use in agricultural areas all over the world to check pests on a variety of crops (Kong *et al.*, 2010). The extensive use of endosulfan leads to water pollution.

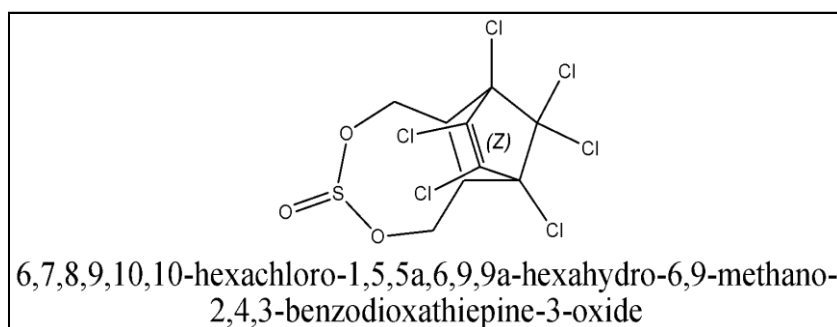


**Figure 2.1: Molecular structure of endosulfan**

Molecular Formula:  $C_9H_6Cl_6O_3S$  and Molecular Weight: 406.9243g/mol.

## 2.2 Endosulfan Toxicity

Endosulfan is biodegradable in nature. *Agrobacterium tumefaciens* bacteria is able to breakdown endosulfan into various residues in the soil (Thangadurai and Suresh, 2014 and Kataoka and Takagi, 2013). However, much of the endosulfan applied in agricultural fields ends up in water bodies. Endosulfan residues can also undergo bioaccumulation and biomagnification. Therefore, Endosulfan can negatively affect non-target organisms including human beings (Kumar *et al.*, 2008 and Thangadurai and Suresh, 2014). Endosulfan has a role as a GABA-gated chloride channel antagonist, inhibits calcium channels and  $Mg^{2+}$  ATPase. It also produces free oxygen radicals in the liver upon ingestion, inhalation or absorption by skin leading to oxidative stress.

Endosulfan concentration in the liver can rise to about 3.4 ppm and is thus converted into a number of water soluble primary metabolites that include endosulfan sulphate, endosulfan diol, endosulfan ether, endosulfan alpha-hydroxy ether and endosulfan lactone. The metabolites accumulate in body tissues causing high lethal effects and significant morbidity. The most common manifestations are neurological disorders although other organ dysfunction also often occurs (Moses and Peter, 2010). A study of electrocardiograms showed that endosulfan poisoning can cause hypotension and other abnormalities (Moses and Peter, 2010). Complications such as hypotension, rhabdomyolysis and hepatic toxicity have also been observed in patients affected by endosulfan as reported in various studies (Kucuker *et al.*, 2009; Mi and Jo, 2009). Endosulfan is absorbed into the body via skin, gastrointestinal tract (ingestion) and through inhalation. This insecticide causes nausea, vomiting, paraesthesia, giddiness, convulsions, coma, respiratory failure, congestive cardiac failure, headache and ataxia.

It can also lead to life threatening metabolic disturbances (Satar *et al.*, 2009). Hepatic, renal and myocardial toxicity, agranulocytosis, aplastic anaemia, cerebral oedema, thrombocytopenia, and skin reaction also have been reported (Ramaswamy *et al.*, 2008). Endosulfan is capable of affecting enzyme activity. Endosulfan has high affinity for thio groups of enzymes and other proteins in a cell, this explains endosulfan toxicity (Sammaiah *et al.*, 2011). Like other pesticides, endosulfan can be transferred from one trophic level to another thus affecting the whole food chain (Ezemonye and Tongo, 2010). It has an estrogenic effect in humans, therefore it can affect the reproductive system and cause reduced sperm production and impaired foetal development. This present study is important since it aims at endosulfan remediation in order to prevent environmental pollution.

### **2.3 Endosulfan and Its Application**

Endosulfan has been extensively used as a pesticide on a variety of crops since 1954 (Li *et al.*, 2009; Verma *et al.*, 2011). Currently, this insecticide is off-patent and has been banned in many countries because of its toxic nature and its persistence in the environment. However, it is still used in some other countries including the United States (Parbhu *et al.*, 2009). In some countries there was an occurrence of health and environmental related issues. For example, it was a cause of concern in British Columbia, where farmers had sprayed it for many years. Other cases were reported in some countries such as India and Cuba where it is still widely used and has caused very dangerous biological effects such as cancer, congenital birth defects, mental, loss of immunity, and neurological disorders as well as reproductive health complications (Wan *et al.*, 2005). In many countries, environmental toxicity of endosulfan remains persistent (Wan *et al.*, 2005), and hence suitable water treatment systems need to be put in place for endosulfan remediation.

### **2.4 Environmental Fate of Endosulfan**

Endosulfan finds its way into water resources majorly by storm water from the fields, leaching and untreated sewage discharge. Much of the endosulfan undergoes biotic and abiotic degradation depending on prevailing environmental conditions (Figure 2.2). It is broken down into compounds such as endosulfan sulphate, endosulfan diol, endosulfan ether, endosulfan alpha-hydroxy ether and endosulfan lactone (Weber *et al.*, 2010; Shivaramaiah and Kennedy, 2006). Endosulfan has a potential for bioaccumulation and biomagnification. Some studies report biodilution occurring at high trophic levels due to increased metabolism (Weber *et al.*, 2010). Because of endosulfan toxicity, its environmental fate is of great concern and therefore water treatment companies and environmental organisations should find it urgent to adopt suitable endosulfan remediation systems.

Endosulfan half-life is 39.5 to 42.1 days. Endosulfan residues dissipate to about 92-97% in the first 4 weeks and by 99% in 238 days from the time of application.

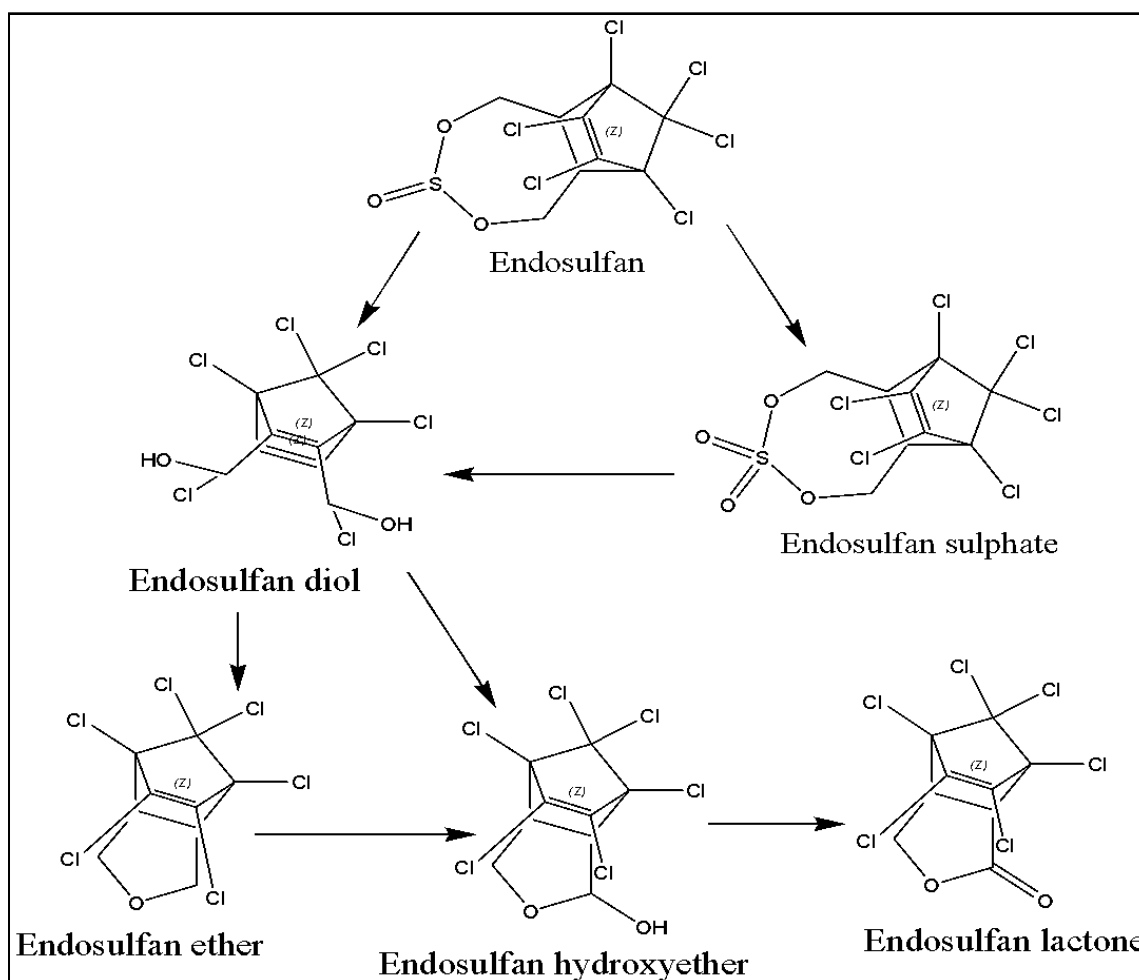


**Figure 2.2: Schematic pathway for endosulfan degradation**

(Source: Shivaramaiah and Kennedy, 2006).

### 2.5 Remediation of Endosulfan from Contaminated Water

A number of research articles have been published in the recent past concerning remediation of endosulfan from contaminated water. Research studies on characteristics of carbon slurry and other novel adsorbent materials for removal of endosulfan from contaminated water, with potential application in curbing environmental risks from such agrochemicals, have been reported (Gupta and Imran, 2008; Crini and Lichtfouse, 2018; Bhatnagar and Minocha, 2006). Elsewhere, Hengpraprom *et al.* (2006) and Polati *et al.* (2006) reported adsorption of pesticides such as  $\alpha$ -endosulfan onto kaolinite particles and to a mixture of kaolinite and montmorillonite particles from aqueous suspension. Craig *et al.* (2015) reports a successful application of biochar/geopolymer structures in remediation of pesticides (such as atrazine, dieldrils, picloram, metalochlor, tebuthiuron and hexazinone) from contaminated water in Australia. A comprehensive study on endosulfan adsorption on hydrophobic zeolites was reported by Yonli *et al.* (2012) and Jiang *et al.* (2018). Recently, geopolymers have shown to

be emerging low cost, sustainable and efficient adsorbents (due to their high adsorption capacities) for removal of various contaminants such as pesticides from water (Shikuku and Sylvain, 2019; Luukkonen *et al.*, 2016; Tomé *et al.*, 2018). Although much research work has been done in terms of remediation of pesticides from contaminated water, no research work has reported the use of MWFA-based geopolymers as adsorbent for endosulfan removal from contaminated water and so recommending an alternative use of the environment polluting MWFA. This work used MWFA-based geopolymers, treated at different sodium silicate to sodium hydroxide mole ratios, as adsorbents for endosulfan removal from contaminated water. Documenting the efficiency of adsorption and the mechanism will contribute to science by providing an understanding about the effect of sodium silicate to sodium hydroxide mole ratio on adsorptive properties of the MWFA-based geopolymers.

## **2.6 Geopolymers**

Geopolymers are a diverse group of ceramic-like materials produced by a geosynthetic reaction of aluminosilicate minerals (Figure 2.3). According to Davidovits (1991), the reactions take place in alkaline solutions at low temperatures, below 100°C. The geosynthetic reaction process goes through a number of geochemical reactions which include mineral dissolution, aluminosilicate polycondensation and structural re-arrangement (Phair *et al.*, 2001). Geopolymers are inorganic, hard and stable at high temperature, inflammable, immobilized and hardened at low temperature. Geopolymers are characterised by a polymeric Si-O-Al framework in which silicon and aluminium alternate in a tetrahedral structure joined together by sharing all the oxygen atoms in three directions. Classification of geopolymers depends on the type of monomeric units involved. This can be classified as:

Polysialate, with (-Si-O-Al-O-) monomer;

Polysialatesiloxo, with (-Si-O-Al-O-Si-O-) monomer;

Polysialatedisiloxo, with (-Si-O-Al-O-Si-O-Si-O-) monomer (Phair *et al.*, 2001).

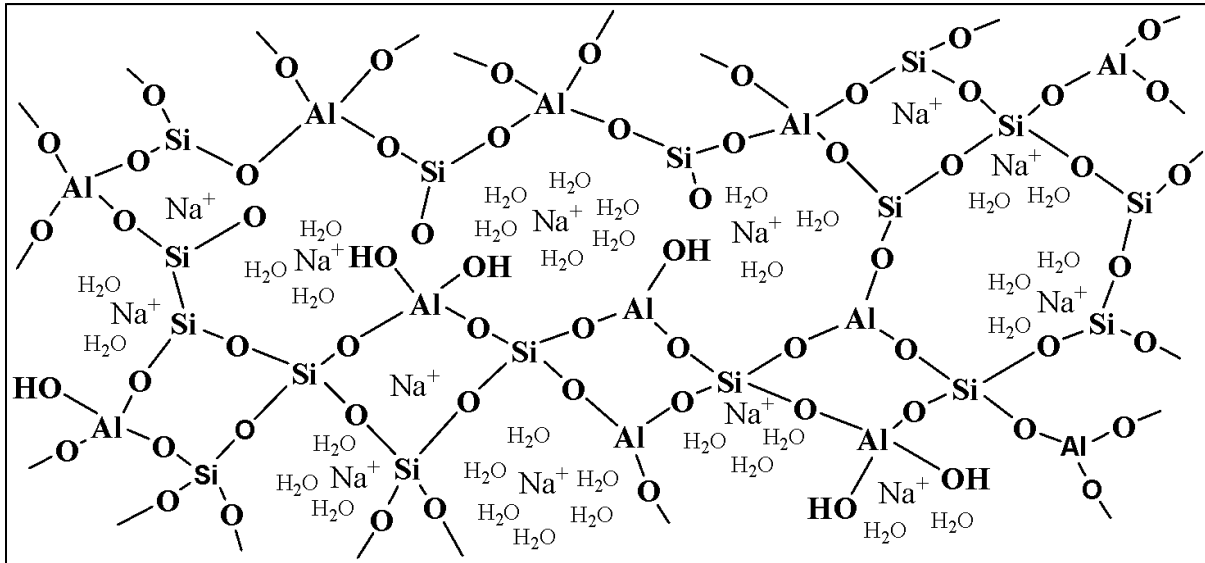


**Figure 2.3: A schematic representation of geopolymer structure**

(Source: Mackenzie and Welter, 2014)

### 2.6.1 Mechanisms of Geopolymer Formation

The geosynthetic reaction that leads to geopolymer formation involves mixing of solid precursors (aluminosilicate sources) with alkaline activator solution (alkali hydroxide and sodium metasilicate). Such aluminosilicate sources may include clay, kaolin, metakaolin, fly ash, volcanic ash and slag. Upon mixing of the aluminosilicate source and alkaline activator solution, the geopolymerization reactions involve:

- i. Glassy aluminosilicate dissolves;
- ii. Dissolved ions diffuse through the reacting mass and reorganise thereby forming small coagulated structures;
- iii. Formation of aluminosilicate gel phases as a result of polycondensation; and
- iv. The aluminosilicate gel transforms to solid state i.e. hardening to form hard solid.

Figure 2-4 provides typical geochemical reactions that leads to formation of different polysialate geopolymers.

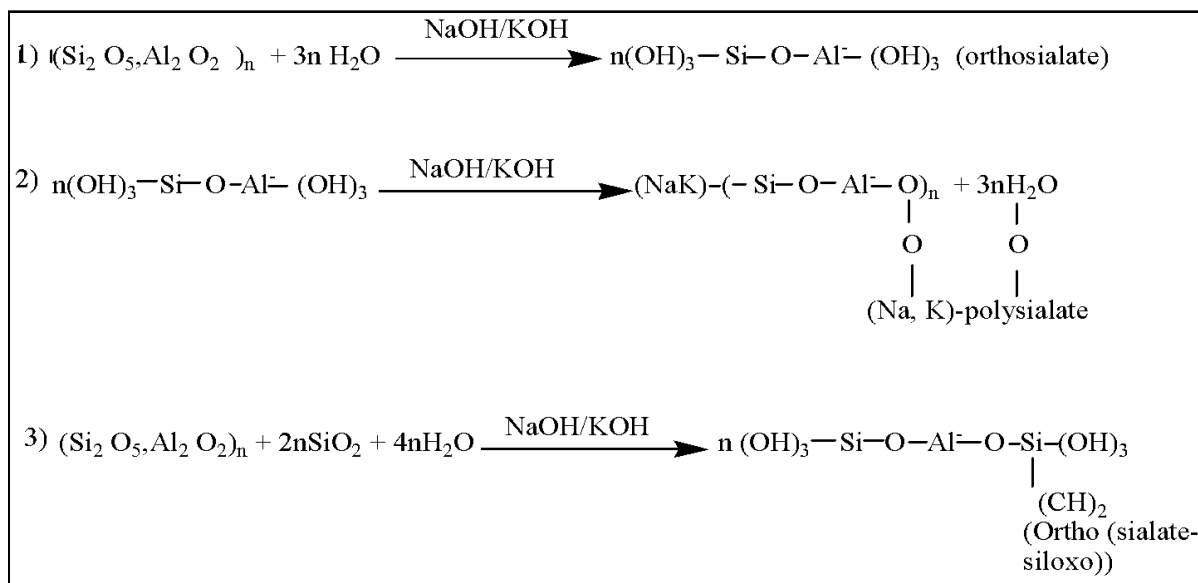


**Figure 2.4: Geopolymerization mechanism**

(Source: Provis and Van Deventer, 2007).

Based on the precursor and synthesis conditions, the rates of geopolymerization reactions, dissolution of aluminosilicate and the mineral phases formed vary significantly. In this work, the mineral phases in the precursor and in the geopolymers will be identified to determine the nature of the geopolymerization process and type of geopolymer formed.

### 2.6.2 Fly ash

Over 80% of fly ash particles have diameters between 0.105-0.154 mm. The mass ratios of particles smaller than 0.063 mm and larger than 0.154 are both lower than 5%. MWFA has a pH of 11 and above. The main elements are Cl, Ca, K, Na, Si, Al, O and S. The main heavy metal elements present in MWFA are Zn, Pb, Cr and Cu. The fly ash exists as irregularly shaped amorphous solids and polycrystalline aggregates. Its leaching toxicity has exceeded the criteria for hazardous wastes (Xinghua *et al.*, 2016; Alba *et al.*, 1997).

### 2.6.3 Fly Ash-Based Geopolymers

Geopolymerization is the process of geopolymer formation. Under alkali activator solution conditions, aluminosilicate source reacts forming an amorphous aluminosilicate with a continuous structure (Van Deventer *et al.*, 2007). The chemical process is called polycondensation exothermic reaction and is based on the reaction involving two materials i.e. alkali activator and reactive aluminosilicate precursor. Geopolymerization greatly depends on the type of alkaline activator present, mostly sodium hydroxide and / or sodium silicate is used (Van Deventer *et al.*, 2007). Fly ash based geopolymers rely on cheap and readily available fly ash as feedstock. For these reasons, there is a growing commercial



potential for fly ash-based geopolymers (Phair *et al.*, 2003). Fly ash geopolymers are anionic with surface area of  $56 \text{ M}^2/\text{g}$  (Li *et al.*, 2006).

Aluminosilicate material with a layered structure and high Al content, is used as an Al-rich source (> 30% Al). A number of compounds have high Al content and are therefore applied during a number of studies. Initially, metakaolin was the single most Al source used but has since been extended to include kaolin (Jaarsveld *et al.*, 1997). Stilbite (Xu *et al.*, 2001) and feldspar (Xu and Van Deventer, 2002) are also possible Al sources. Content analysis shows that a typical fly ash-based geopolymer may consist of about 60% dry mass fly ash, dry mass Al- additive of approximately 12% and about 28% alkali activator (Phair and Van Deventer, 2002a; Swanepoel and Strydom, 2002).

The structural, textural, and mechanical properties of a geopolymer adsorbent is affected by its composition and synthesis conditions, including the type of alkali cation (M), the humidity, the temperature and the Si/Al,  $\text{M}_2\text{O}/\text{H}_2\text{O}$ , and  $\text{M}_2\text{O}/\text{SiO}_2$ , ratios. The ratio of alkali activator and aluminosilicate source used during mixing plays a significant role in forming a geopolymer having particular mechanical and microstructural properties. Previous studies recommend a Si/Al composition between 2.5 and 3.5 (Xu, and Van Deventer, 2002; Swanepoel and Strydom, 2002). Ibrahim *et al.* (2022) used 2.5 as ratio of sodium silicate to sodium hydroxide. Activated charcoal, fly ash, metakaolin, dolomite are among few materials used as adsorbent for toxic metals ions and organic molecules in water treatment. Fly ash can be a by-product of industrial combustion of coal. Such fly ashes collect on electrostatic separators and consist of unburned carbon particles and aluminosilicate particles.

Fly ash may also be a municipal waste incineration by-product. They are particles with pozzolanic properties and the mineral constituents include glassy phase and minor crystalline phases (quartz, mullite, hematite and magnetite). Current global production is 500 million tons annually (Dwivedi and Jain, 2014). The most common way of managing fly ash is to dispose it in landfills but this is not an environmentally friendly solution (Qiu *et al.*, 2019). The amount of MWFA that must be discarded in landfills will be reduced tremendously through alternative use. It is generally considered that fly ash has an immense potential as feed stock in various industrial applications including synthesis of binders and geopolymers (Hardjito *et al.*, 2005; Patankar *et al.*, 2015). Fly ash is preferred because of low cost and availability. Furthermore, geopolymerization provides an environmentally friendly solution to fly ash pollution. Fly ash-based geopolymers are important in remediation of hazardous

organic molecules such as dyes, organic agrochemicals and toxic elements such as Ba, Cd, Co, Cu, Nb, Hg, Pb, Sn and U. The toxic molecules and elements can be tightly fixed in the three-dimensional geopolymer matrix structure. This property may be applied in water treatment to remove hazardous chemicals from contaminated water.

It has been reported in previous studies that small variations in compositional factors such as pH, the nature of the setting additive (Ca rich source) and alkali activator leads to considerable variation in adsorption properties of the resultant fly ash-based geopolymers such as metal immobilisation within its structure (Phair and Van Deventer, 2001; Sumajouw and Rangan, 2006). The NaOH concentration used should be within recommended range as higher molarity of NaOH solution that is above 10 M, causes a decrease in the mechanical strength of the fly ash geopolymer (Abdullah *et al.*, 2018; Kawade *et al.*, 2016; Nath and Sarker (2017). Concentration of NaOH solution has strong influence on strength of geopolymer formed since NaOH molarity will affect the linking of aluminosilicate geopolymer network. In addition, there is a change in the microstructure of the geopolymer material since some loss in mechanical properties may occur due to the free OH<sup>-</sup> in the alkali-activated matrix (Chang, 2009; Daud *et al.*, 2021). Consequently there are changes in the properties of the end product. Some studies reported that the type and concentration of alkali activator affected the properties of resulting geopolymers (Abdullah *et al.*, 2011; Abdullah *et al.*, 2018). Higher alkali activator content gives a higher compressive strength. The most common alkali activator used in geopolymerization is sodium hydroxide. It is sometimes combined with sodium silicate.

In this study, material properties such as mineralogy, morphology, and functional groups rearrangement were investigated. Through examining of the material properties of the starting material, explanation on the synthesized material and the adsorption properties of the geopolymer can be given as a function  $\text{Na}_2\text{SiO}_3$  concentration in alkaline activator. In this work, three samples of MWFA-based geopolymers, prepared using alkaline activator solutions with different silica content, were synthesized, characterised and investigated for their adsorption performance for aqueous endosulfan. The effect of sodium silicate to sodium hydroxide mole ratio on the structure and composition of the geopolymers formed was also investigated. MWFA being an environmental nuisance, its application in geopolymerization offers its eradication strategy.

This research work contributed to science by establishing an understanding on the effect of change of mole ratio of sodium silicate to sodium hydroxide on material properties and adsorption performance of the MWFA-based geopolymers. The alternative use of the environmental pollutant, MWFA, for geopolymer synthesis and its subsequent application in endosulfan remediation is helpful in management of MWFA by the municipalities, environmental organisations and water treatment companies.

## CHAPTER THREE

### MATERIALS AND METHODS

The methods used throughout the study are outlined in this chapter. The reagents used, instruments and experimental set-ups are described.

#### 3.1 Materials and Chemicals

Municipal waste fly ash (MWFA) was randomly collected from Environmental Combustions and Consultancy Limited, Migori, Kenya. Some 90 g of MWFA was crushed, sieved using a 100  $\mu\text{m}$  pore size sieve, and stored in a vacuum desiccator. Analytical reagent (AR) grade sodium silicate ( $\text{Na}_2\text{SiO}_3 \cdot 9\text{H}_2\text{O}$ ), sodium hydroxide (NaOH), endosulfan (6, 9 -Methano - 2, 4, 3 - benzodioxathiepin, 6, 7, 8, 9,10,10 - hexachloro-1, 5, 5a, 6, 9, 9a – hexahydro -3, 3-dioxide), hydrochloric acid (HCl) and sodium chloride (NaCl) were purchased from Kobian Scientific Limited, Kenya.

#### 3.2 Methodology

##### 3.2.1 Synthesis of the Geopolymer Adsorbents

A 50 mL solution of 8 M NaOH was prepared in a polypropylene beaker using a magnetic stirrer. Three, 15 mL portions of the 8 M NaOH solution were transferred into three different polypropylene beakers labelled A, B, and C and to them, 5.81 g, 6.98 g, and 8.14 g of sodium silicate were added, corresponding to 0.17, 0.21 and 0.24 sodium silicate to sodium hydroxide mole ratios, respectively. The activator solutions were stirred at 800 rpm and at a temperature of 40 °C for 30 minutes to obtain homogeneous mixtures. The activator solutions were kept covered with parafilm to prevent carbonation and allow for complete de-polymerization of sodium silicate for 24 hours.

Activator solutions were mixed with municipal waste-fly ash (MWFA) at a solid-to-liquid (S/L) ratio of 2 and shaken (Shaking Incubator, Model: SSI10R-2, Orbital-Shaking, Infitek Co., Ltd., Jinan, China) for 5 minutes at 150 rpm to form pastes. The fly ash-based geopolymer pastes were transferred into cylindrical containers and then cured in an oven (FC-1000, AS ONE, Blast Constant-Temperature Drying Oven Robust Type, Hanoi, Vietnam) at 25 °C for 24 hours. The three cured geopolymers that is MWFA-based geopolymer A (GPA), MWFA-based geopolymer B (GPB), and MWFA-based geopolymer C (GPC) were then crushed using mortar pestle set and sieved through a 100  $\mu\text{m}$  sieve, and stored in a desiccator before use (El Alouani *et al.*, 2018).

### 3.2.2 Characterization of the Geopolymer Adsorbents

Characterization followed standard methods. The scanning electron microscope (SEM) (ZEISS EVO L 15, Zeiss Group, Cologne, Germany) operating at 20 kV accelerating voltage was used to carry out morphology and microstructure analyses while energy dispersive X-ray (EDX) analyses were carried out using an Oxford make EDX detector (Xplore TEM-80 mm<sup>2</sup>, Oxford, England) to obtain the percentage elemental composition of the geopolymers and MWFA. The X-ray diffraction (XRD) was used to determine mineralogical composition of the geopolymers and MWFA. The diffractograms were generated using an X-ray Powder Diffractometer (Bruker D8 Discovery, Bruker Corporation, Billerica, Massachusetts, United States of America) with the Bragg-Bretano theta-theta configuration in the 2 $\theta$  range from 6° to 80° with a step of 0.02° and 1 s per step scan rate and the CuK $\alpha$  radiation at 27.5 kV and 25 mA. The degree of crystallinity (DOC) of the geopolymers and MWFA was computed as the ratio of the area of the crystalline peaks to the total sum of areas of peaks for both amorphous and crystalline phases using OriginPro 9.0 software. The determination of the functional groups of the geopolymers and MWFA was identified using Fourier Transform Infrared spectroscopy (FTIR). The IR spectra were collected using (Cary 630 FTIR, Agilent Technologies, Santa Clara, California, United States of America) and (PerkinElmer Spectrometer 100, Waltham, Massachusetts, United States of America). The pH point of zero charge (pH<sub>pzc</sub>) of MWFA and the synthesized geopolymers was determined using the pH drift method (Dzoujo *et al.*, 2022; Hermann *et al.*, 2022). To 20 mL of 0.1 M NaCl solutions of pH between 2 and 12, 0.1 g of adsorbent samples were introduced and stirred, then kept at room temperature for 8 h after which the final pH values of the solutions were recorded with a pH meter (VOLTCRAFT PH-100ATC, Voltcraft, Hirschau, Bavaria, Germany).

### 3.2.3 Adsorption Experiments

Adsorption experiments were conducted in batch-mode. The initial endosulfan concentrations used in the adsorption experiments were 0, 4, 8, 12, 16, and 20 mg/L. The equilibration contact time, pH, temperature, and adsorbent dosage were kept constant at 90 minutes, pH 5, 303 K, and 0.1 g/50 mL endosulfan solution, respectively. After equilibration, the mixtures were filtered and the residual endosulfan concentration in the filtrate was determined spectrophotometrically at  $\lambda_{\max} = 212 \text{ nm}$  using a UV-visible spectrophotometer (MERCK spectroquant Pharo 300 UV/visible instruments, Merck KGaA, Darmstadt, Germany).

The amount of endosulfan adsorbed at equilibrium, mg/g, was calculated as:

$$q_e = \frac{(C_i - C_e)V}{M} \quad 3-1$$

where  $C_i$  and  $C_e$  are the initial and equilibrium endosulfan concentrations (mg/L), respectively.  $V$  is the volume, L, of the solution and  $m$  is the mass, g, of the adsorbent.

Adsorption removal efficiency ( $\eta$ ) at equilibrium time was calculated as:

$$\eta = \left[ \frac{C_i - C_f}{C_i} \right] \times 100 \quad 3-2$$

where  $C_i$  and  $C_f$  were the initial concentration and final concentration, respectively.

Additionally, the effect of pH was investigated in the pH range of 2.0 - 10.0. Adsorbent dosage, contact time, initial endosulfan concentration, and temperature were kept constant at 0.1 g/50 mL solution, 90 minutes, 8 mg/L, and 303 K, respectively. A 0.1 M HCl and 0.1 M NaOH were used to adjust the pH of the solution accordingly.

The effect of contact time was studied at predetermined intervals of 0, 10, 20, 30, 40, 50, 60, 90, 120, and 150 minutes. Adsorbent dosage, pH, initial endosulfan concentration, and temperature were kept constant at 0.1 g/50 mL solution, pH 5, 8 mg/L, and 303 K, respectively. An aliquot of the supernatant was then drawn-out to determine residual endosulfan.

The amount of endosulfan adsorbed ( $q_t$ ) onto the geopolymers at any given time, ( $t$ ), was given by:

$$q_t = \frac{(C_i - C_t)V}{M} \quad 3-3$$

Where  $C_t$  is the adsorbate concentration (mg/L) at any given time

To investigate the effects of temperature, the adsorption processes were studied to establish its thermodynamic characteristics in the temperature range of 303-353 K in a temperature-controlled shaker at 150 rpm (Shaking Incubator, Model: SSI10R-2, Orbital-Shaking, Infitek Co., Ltd., Jinan, China) for a stipulated fixed duration. Contact time, pH, initial endosulfan concentration, and geopolymer dosage were kept constant at 90 minutes, pH 5, 8 mg/L, and 0.1 g/50 mL solution, respectively.

Adsorbent dosage was also investigated where different amounts of adsorbent, ranging from 0.05-0.3 g, were used in 50 mL of endosulfan solution. Contact time, pH, initial endosulfan concentration, and temperature were kept constant at 90 minutes, pH 5, 8 mg/L, and 303 K, respectively.

### 3.2.4 Adsorption Kinetics

In most studies, time dependent data is fitted to *pseudo*-first-order and *pseudo*-second-order models in order to determine the reaction rates, order of adsorption reaction and nature of the rate-controlling step (Al-Ghouti *et al.*, 2020; Polati *et al.*, 2006).

The adsorption-desorption kinetics of endosulfan on commercial activated carbon and activated sawdust carbon has been assessed in previous studies (Kakoi *et al.*, 2015). The data was fitted on the linear *pseudo*-first order and *pseudo*-second order models. A conclusion were made that the adsorption data was best described by *pseudo*-second order models.

El Alaouani *et al.* (2018) obtained various kinetic parameters for the chemisorption of cationic dye (methylene blue) onto fly ash-based geopolymer. The adsorption data were fitted on linear *pseudo*-first order kinetics and the *pseudo*-second- order. On the basis of correlation coefficients i.e.  $0.99 \leq R^2 \leq 1$ , the experimental data were best fitted on *pseudo*-second order rate model. Also, the experimental amount sorbed at equilibrium (mg/g),  $q_e$ , was close to the calculated,  $q_e$ , which supported the finding that *pseudo*-second order model fit best with experimental data. However, information on half-life ( $t_{1/2}$ ) and initial sorption rate ( $S_{rate}$ ) was not reported.

The adsorption kinetics for endosulfan onto the geopolymers were analyzed using Lagergren *pseudo*-first-order (PFO) (equation 3-4) (Yuh-Shan, 2004) and *pseudo*-second-order (PSO) (equation 3-7) (Ho and McKay, 1999) kinetic models.

$$q_t = q_e(1 - e^{-k_1 t}) \quad \text{Error! No text of specified style in document.-4}$$

where  $k_1$  is the PFO rate constant ( $\text{min}^{-1}$ ),  $q_e$  (mg/g) is the adsorption capacity at equilibrium, and  $q_t$  (mg/g) is the adsorbed amount of adsorbate at any given time (minutes). In PFO kinetics, the initial adsorption rate and adsorption half-life were calculated using equations 3-5 and 3-6, respectively.

$$S_{rate} = k_1 q_e \quad \text{Error! No text of specified style in document.-5}$$

$$t_{1/2} = \frac{\ln 2}{k_1} \quad \text{Error! No text of specified style in document.-6}$$

The *pseudo*-second-order kinetic model is given as:

$$q_t = \frac{q_e^2 k_2 t}{1 + k_2 q_e t}$$

*Error! No text of*

*specified style in document.-7*

where  $k_2$  is the PSO rate constant (g/mg/min).

The initial sorption rate ( $S_{rate}$ ) and the adsorption half-life ( $t_{1/2}$ ) for PSO were obtained from equations 3-8 and 3-9, respectively, (Ho and McKay, 1999). The computed values are presented in Table 4-4.

$$S_{rate} = k_2 q_e^2$$

*Error! No text of*

*specified style in document.-8*

$$t_{1/2} = \frac{1}{k_2 q_e}$$

*Error! No text of*

*specified style in document.-9*

From literature, the required contact time for initial endosulfan concentration (10-20 mg/L) to get to equilibrium state was 1-3 hours while that of higher concentration (30-40 mg/L) is 4-5 hours (Kakoi *et al.*, 2015). Adsorption of a solute onto a porous adsorbent involves three consecutive steps of mass transport (Fytianos *et al.*, 2000). The adsorbate moves through the solution, that is, film diffusion, followed by migration of solute molecules from the particle surface into interior sites by pore diffusion and finally the adsorbate is adsorbed into the adsorbent's active sites. This process takes relatively long contact time. Film diffusion, pore diffusion, and the amount of agitation applied in the system control rate of adsorption. Kakoi *et al.*, 2015 reported optimum agitation rate to be 200 rpm. If relatively little agitation occurs between the geopolymer particle and the adsorbate solution, the surface film of the liquid around the particle will be thick and film diffusion becomes the rate-limiting step. However, with adequate agitation, the rate of film diffusion increases until pore diffusion generally becomes the rate-limiting step (Kakoi *et al.*, 2015).

### 3.2.5 Thermodynamic Parameters of Adsorption Process

The effect of varying temperature while other environmental conditions are kept constant gives the thermodynamic aspect of the adsorption experiment. Data obtained from varying temperature were used to determine the thermodynamic nature of the adsorption process such as feasibility, reversibility or irreversibility of the experiment. Change in Gibbs free energy,  $\Delta G$ , ( $\text{kJmol}^{-1}$ ) of the adsorption process is normally calculated using equations 3-10 and 3-11.

$$\Delta G = \Delta H - T\Delta S$$

**3-10**



Where  $\Delta G$  is change in Gibbs free energy ( $\text{kJmol}^{-1}$ ),  $\Delta H$  is change in enthalpy ( $\text{kJmol}^{-1}$ ),  $\Delta S$  is change in entropy ( $\text{JK}^{-1}\text{mol}^{-1}$ ),  $T$  is the absolute temperature (Kelvin).

$$\boxed{\Delta G = -RT \ln K_c} \quad 3-11$$

where  $K_c$  is the dimensionless equilibrium constant,  $T$  is the absolute temperature (Kelvin) and  $R$  is the universal gas constant ( $8.314 \text{ J/mol. K}$ ).

$$\boxed{K_c = 1000K_d} \quad 3-12$$

where  $K_d$  is the distribution coefficient ( $\text{L/g}$ ) when the density of water is  $1000 \text{ g/L}$  (Hermann *et al.*, 2022).

$$\boxed{K_d = \frac{C_{ads}}{C_e}} \quad 3-13$$

$K_d$  is the distribution coefficient ( $\text{L/g}$ ).  $C_{ads}$  represents the equilibrium endosulfan concentration in the solid phase ( $\text{mg/g}$ ) and  $C_e$  is the equilibrium endosulfan concentration in the solution ( $\text{mg/L}$ ) (Hermann *et al.*, 2022).

Enthalpy change,  $\Delta H$ , ( $\text{kJmol}^{-1}$ ) and change in entropy,  $\Delta S$ , ( $\text{JK}^{-1}\text{mol}^{-1}$ ) of the adsorption process is normally calculated using the Van't Hoff equation 3-14.

$$\boxed{\ln K_c = \frac{\Delta S}{R} - \frac{\Delta H}{RT}} \quad 3-14$$

where  $K_c$  is the dimensionless equilibrium constant,  $T$  is the absolute temperature (Kelvin) and  $R$  is the universal gas constant ( $8.314 \text{ J/mol. K}$ ).

The Van't Hoff equation [3-14] describes the temperature dependence of  $K_c$  by relating ( $\Delta G$ ) to  $K_c$ . When  $K_c = 1$  then ( $\Delta G$ ) = 0 and the process is at equilibrium.  $K_c < 1$  then ( $\Delta G$ ) is positive and the process is non spontaneous.  $K_c > 1$  then ( $\Delta G$ ) is negative and the process is spontaneous. The decrease in  $\Delta G$  values with an increase in temperature implies that the adsorption process is increasingly spontaneous, a phenomenon characteristic of an endothermic process. The low magnitudes of  $\Delta G$  values suggest a physisorption mechanism (Dzoujo *et al.*, 2022).

Change in Gibb's free energy ( $\Delta G$ ) will tell the feasibility of the process, whether the reaction will tend to proceed in the forward or reverse direction that is, favourable or unfavourable. If ( $\Delta H$ ) is positive then the adsorption process is endothermic and if ( $\Delta H$ ) is negative then the reaction is exothermic. Enthalpy change ( $\Delta H$ ) will tell whether the process is endothermic or exothermic. Change in entropy ( $\Delta S$ ) will tell the spontaneity of the adsorption process.

Dzoujo *et al.* (2022) reported positive enthalpy ( $\Delta H$ ) values for the adsorption of the methylene blue on the geopolymer-biochar composites adsorbents which indicated an endothermic process. The positive values of change in entropy ( $\Delta S$ ) indicated an increased disorderliness at the solid/liquid interphase. The  $\Delta H$  values, less than 40 kJ/mol, confirmed that the adsorption of methylene blue onto the geopolymer-biochar composites is a physical process (Shikuku and Jemutai-Kimosop, 2020). The thermodynamics data indicate that the adsorption of methylene blue onto the geopolymer-biochar composites is entropy-driven. Methylene blue, being a large organochlorine molecule, gives insights on the mechanism of adsorption endosulfan onto geopolymers.

### 3.2.6 Adsorption Isotherm Modelling

Isotherm models were useful in predicting the equilibrium distribution of the solute. In most studies, two or more adsorption isotherm studies were applied and then a conclusion was made on which isotherm model best described the adsorption data. In this study Langmuir and Freundlich adsorption isotherm models were adopted on the geopolymers to tell the nature of adsorption process by varying the initial endosulfan concentration and fitting on the isotherm models. The use of Langmuir and Freundlich adsorption isotherm models could give more precise inference on whether the adsorption was monolayered or multi-layered.

#### 3.2.6.1 Langmuir Isotherm Model

Langmuir isotherm model assumes that, there occurs a single layer adsorption of adsorbate molecules onto a fixed number of active sites and that there's no lateral interaction between adsorbed molecules on a morphologically homogeneous surface. The adsorption sites, in this case, are considered to be identical (Meroufel *et al.*, 2013). The theoretical monolayer maximum adsorption capacity of the adsorbent and the correlation coefficients obtained are used to determine the best-fitting model for the adsorption data.

El Alaouani *et al.* (2018) found that Langmuir model best described the adsorption data among other three adopted models. In their study, they obtained Langmuir maximum adsorption capacity and the separation factor,  $R_L$ , which is a dimensionless equilibrium constant that indicates the shape of the isotherm. The  $R_L$  value relates to the nature and feasibility of the adsorption isotherm as summerized in Table 2-1 (Meroufel *et al.*, 2013). Similar studies on adsorption of various adsorbates such as sodium dodecyl benzene sulfonate (SDBS), onto fly ash-based geopolymers reported Langmuir model as best-fitting model for the adsorption data (Siyal *et al.*, 2019). The use of Langmuir and Freundlich

adsorption isotherm models can give more precise inference on whether the adsorption process was physisorption or chemisorption. This will then provide an understanding on whether or not, sodium silicate to sodium hydroxide ratio has a bearing on the adsorption mechanism.

**Table 3.1: Interpretation of Langmuir separation constant,  $R_L$**

$R_L$ Value	Adsorption process
$R_L = 1$	Linear
$R_L > 1$	Not favourable
$R_L = 0$	Not reversible
$0 < R_L < 1$	Favourable

**Source: Meroufel *et al.*, 2013**

### 3.2.6.2 Freundlich Isotherm Model

The Freundlich model proposes a multilayer adsorption (Halsey, 1948; El Alaouani *et al.*, 2018). This kind of adsorption has differing dispersion of adsorption affinities onto the heterogeneous surface of the adsorbent without lateral interaction. In line with this postulate, the adsorption sites which are energetically favoured are occupied first, followed by those having diminishing binding energies with increasing rates of site occupancy (El Alaouani *et al.*, 2018).

The Freundlich equation is exponential and therefore the amount of adsorbate on the adsorbent surfaces rises with increase in solute concentration. A coefficient of determination ( $R^2$ ) value is close to unity shows a good fit between this model and the experimental data (Halsey, 1948; El Alaouani *et al.*, 2018). If the data was better described by Freundlich model, there was a high likelihood that the adsorption process is chemisorption.

### 3.2.7 Statistical Analysis

Variability between replicates was expressed in terms of error bars. The statistical difference was tested using One Way Analysis of Variance on OriginPro 9.0 software as presented in the appendices 1, 2 and 3.

## CHAPTER FOUR

### RESULTS AND DISCUSSION

This chapter describes the results obtained from the various sample treatments from adsorbents characterization to sorption kinetics, thermodynamics parameters and isotherms. Herein discussed are the physical and chemical meaning and interpretations.

#### 4.1 Production of the Geopolymers

The MWFA had coarse profile with a mixture of very fine and rough particles. Effervescence is observed during the reaction between MWFA and alkaline activator solution and the MWFA-based geopolymers synthesized appeared to have numerous pores distributed throughout the whole mass, similar to pumice rocks, as shown in Figure 4.1. Porosity increases from GPA, to GPB to GPC with increase in sodium silicate to sodium hydroxide mole ratio.



**Figure 4.1: Photographs of MWFA, GPA, GPB, and GPC (Scale - 3:4)**

## 4.2 Characterization Studies of the MWFA and MWFA-based Geopolymers

### 4.2.1 Functional Group Identification

FTIR plots (Figure 4.2) present the functional groups present in MWFA.

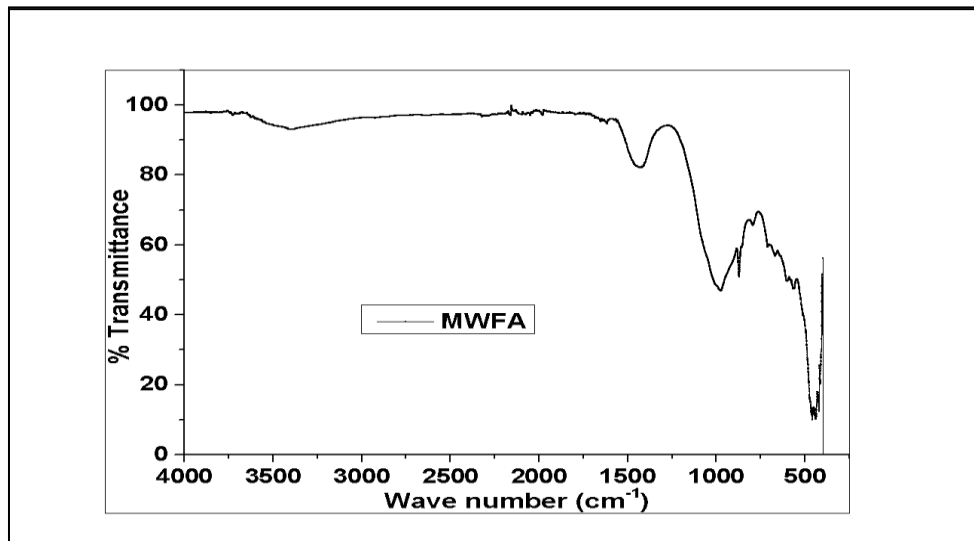


**Figure 4.2: FTIR spectrum of MWFA**

For MWFA, there were absorption bands at  $1616\text{ cm}^{-1}$ ,  $3400\text{ cm}^{-1}$ ,  $1435\text{ cm}^{-1}$ , and a pre-eminent band at  $989\text{ cm}^{-1}$  corresponding to deformation and stretching vibrations of  $\text{-OH}$ ,  $\text{H-O-H}$ ,  $\text{C=O}$  bonds,  $\text{Si-O-T}$  (T-tetrahedral Al or Si) bonds. Other important bands were centered between  $400\text{ cm}^{-1}$  and  $800\text{ cm}^{-1}$  wave numbers corresponding to asymmetric and symmetric stretch vibrations of aluminosilicate tetrahedral. Similar results were reported by Innocenzi et al. (2003) in which the silica bands appeared in the  $1000\text{--}1300\text{ cm}^{-1}$  region.

FTIR plots (Figure 4.3) present the functional groups found in MWFA and the MWFA-based geopolymers.

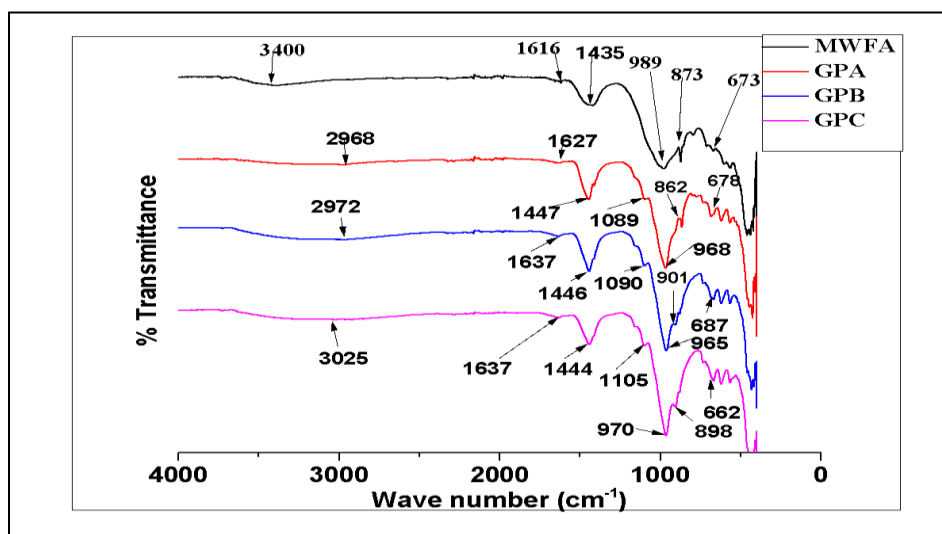


**Figure 4.3: FTIR spectra of MWFA, GPA, GPB, and GPC**

A comparison of MWFA-based geopolymers with MWFA shows some changes in the bands. The presence of quartz in MWFA gave Si-O-T (T-tetrahedral Al or Si) bonds responsible for the band at  $989\text{ cm}^{-1}$  (Siyal *et al.*, 2019). The shift in this band to lower wavenumbers ( $968\text{ cm}^{-1}$ ,  $965\text{ cm}^{-1}$ ,  $970\text{ cm}^{-1}$ ) in the MWFA-based geopolymers GPA, GPB, and GPC show that some quantity of metasilicate participated in the geopolymerization reaction.

The bands at  $989\text{ cm}^{-1}$  and  $673\text{ cm}^{-1}$  correspond to the asymmetric and symmetric stretch vibrations of aluminosilicate tetrahedral, Si-O-T (T-tetrahedral Al or Si) in MWFA. The asymmetric stretch vibration bands reduced to lower wavenumbers ( $968\text{ cm}^{-1}$ ,  $965\text{ cm}^{-1}$ , and  $970\text{ cm}^{-1}$ ), increased in intensity, and narrowed with the synthesis of GPA, GPB, and GPC, respectively. According to Daud *et al.* (2021), Si-O-T gives the main band used as evidence of geopolymer synthesis. During geopolymerization, there is bond breaking and bond formation responsible for the variations in the main band (Siyal *et al.*, 2016). The shift in these main bands to lower wavenumbers was evidence that changes occurred in the angle and length of the Si-O-Si bonds indicating that the sodium silicate to sodium hydroxide mole ratio contributes significantly to the structure of the prepared geopolymers (Innocenzi, 2003).

The bands at  $1616\text{ cm}^{-1}$  and  $3400\text{ cm}^{-1}$  in the MWFA are due to deformation and stretching vibrations of  $\text{-OH}$  and  $\text{H-O-H}$  bonds (Zhang *et al.*, 2012). The stretching vibrations of  $\text{H-O-H}$  and  $\text{-OH}$  bands appear at  $2968\text{ cm}^{-1}$ ,  $2972\text{ cm}^{-1}$ , and  $3025\text{ cm}^{-1}$  for GPA, GPB, and GPC respectively. The deformation vibrations of  $\text{-OH}$  bands appear at  $1627\text{ cm}^{-1}$ ,  $1637\text{ cm}^{-1}$ , and  $1637\text{ cm}^{-1}$  for GPA, GPB, and GPC respectively. The  $\text{H-O-H}$  and  $\text{-OH}$  bond bands indicate the presence of water and silanol groups (Tome *et al.*, 2018). The silanol group and water molecules trapped in the geopolymer hollows are responsible for the shifts in the deformation vibrations of  $\text{-OH}$  bands to higher wavenumbers (Zhang *et al.*, 2012; Liu *et al.*, 2016). Previous related geopolymer studies also reported similar trends in FTIR analysis, confirming the successful synthesis of geopolymers GPA, GPB, and GPC (Sarkar *et al.*, 2017; Nath and Sarker, 2017).

#### **4.2.2 Morphological and Composition Analysis**

The morphological and structural analysis of the MWFA obtained from SEM-EDX images are shown in Figure 4.4. MWFA appears to have loosely packed structures with high porosity.

This is consistent with the findings of El Alouani *et al.* (2018) which reported loosely packed and porous structures.

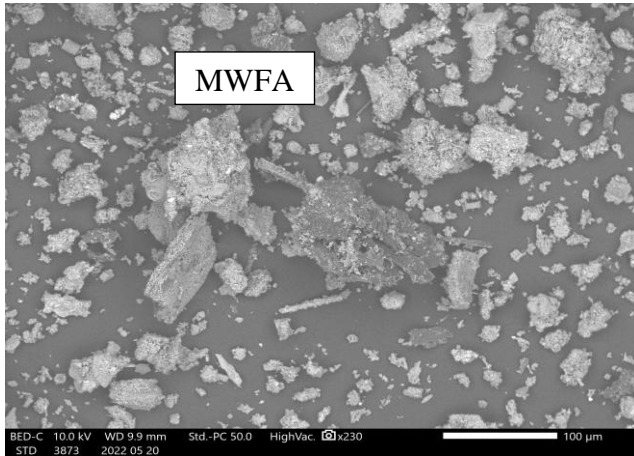


**Figure 4.4: SEM image of MWFA (X230)**

The percentage elemental composition of the MWFA are shown in Table 4-1. The Si/Al ratio in MWFA was found to be 1.18. Sodium was below detection limits since alkaline activator had not been added. Presence of Al and Si makes MWFA a good precursor for geopolymerization.

**Table 4.1: Elemental composition of precursor (MWFA)**

	O (%)	Mg(%)	Na (%)	Al (%)	Si (%)	Ca (%)	Si/Al
MWFA	56.84	2.26	ND*	8.34	9.84	23.08	1.18

**\*ND –not detected**

The morphological and structural analysis of the MWFA, GPA, GPB, and GPC obtained from SEM-EDX images are shown in Figure 4.5. One clear observation is the uniform granular, tiny, spherical, and loosely packed structures in the geopolymers, evidence that geopolymerization occurred (Maleki *et al.*, 2019; El Alouani *et al.*, 2018). The absence of tinny spherical structures in GPA, GPB, and GPC indicates almost complete geopolymerization of the precursor materials into geopolymers. Comparatively, the spongy and gel-like morphology is more elaborate in GPC and GPB than in GPA (Al-Ghouti *et al.*, 2020). The presence of pores and cavities on the surfaces of the adsorbents is the key factor for endosulfan removal from wastewater by adsorption (Shokrollahi *et al.*, 2011; Ghani *et al.*, 2020).

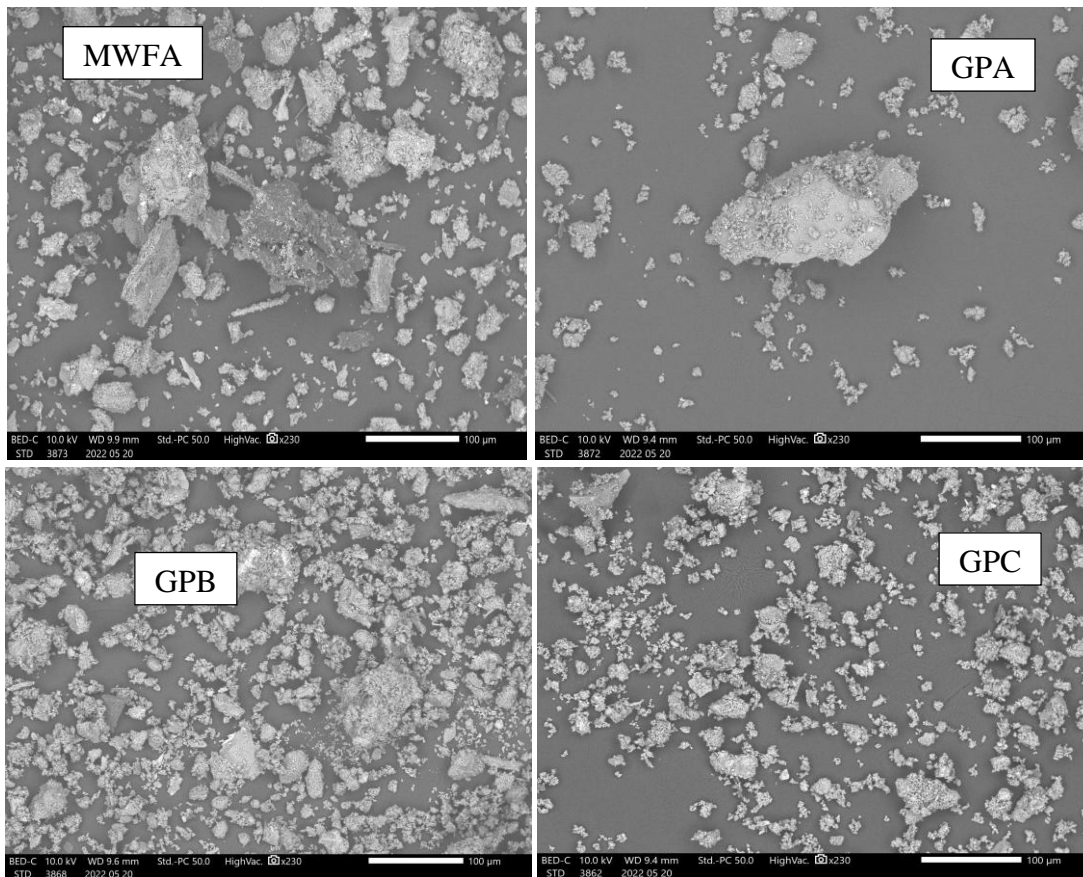


**Figure 4.5: SEM images of MWFA, GPA, GPB, and GPC at X230 magnification**

The percentage elemental composition of the MWFA and the prepared geopolymers are shown in Table 4.2. The Si/Al ratio in MWFA and the geopolymers was found to be different. The changes in elemental composition arose from the alkaline activator solutions used. The MWFA-based geopolymers had Si/Al ratio lower than 2.4 indicating that they had polysialate-siloxo (-Si-O-Al-O-Si-O-) structure (El Alouani *et al.*, 2018). The amount of heavy metals in the MWFA and the MWFA-based geopolymers was undetectable, indicating the unlikely possibility of secondary pollution from the adsorbents (Ghani *et al.*, 2020).

**Table 4.2: Elemental composition of MWFA-based geopolymers**

	O (%)	Mg (%)	Na (%)	Al (%)	Si (%)	Ca (%)	Si/Al
MWFA	56.84	2.26	ND	8.34	9.84	23.08	1.18
GPA	61.83	ND	25.78	3.36	6.41	2.62	1.91
GPB	55.29	ND	19.40	8.65	16.66	ND	1.93
GPC	53.86	ND	22.76	7.77	15.61	ND	2.01

**KEY:**

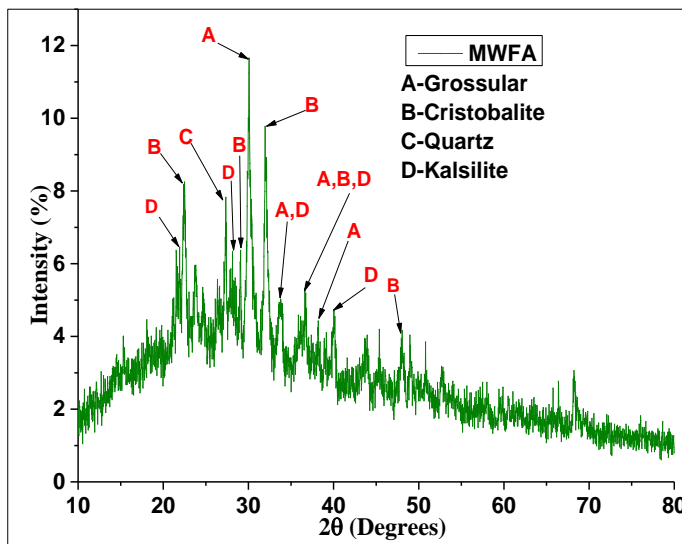
ND- not detected



### 4.2.3 Crystallinity and Mineralogical Studies

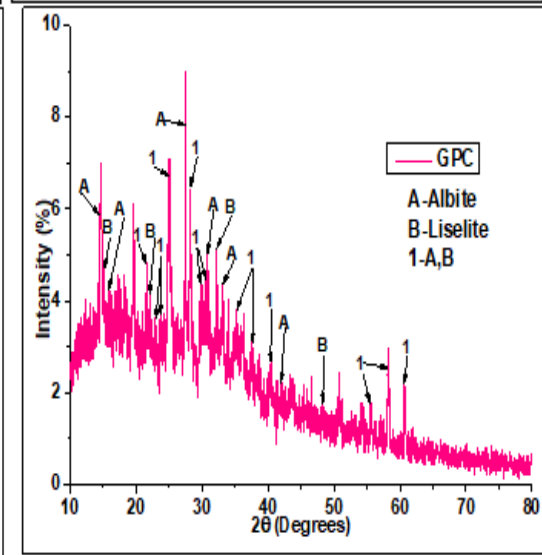
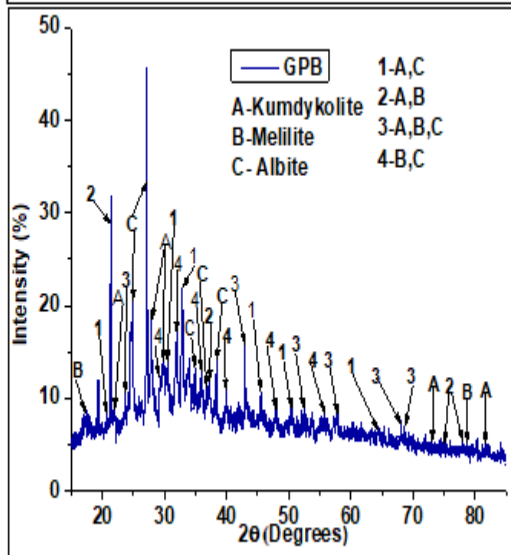
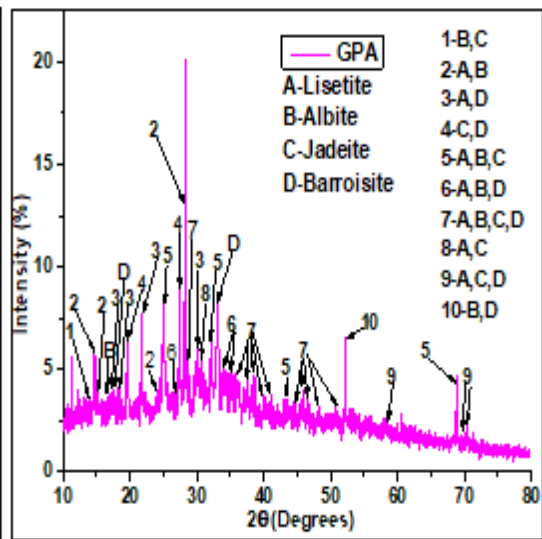
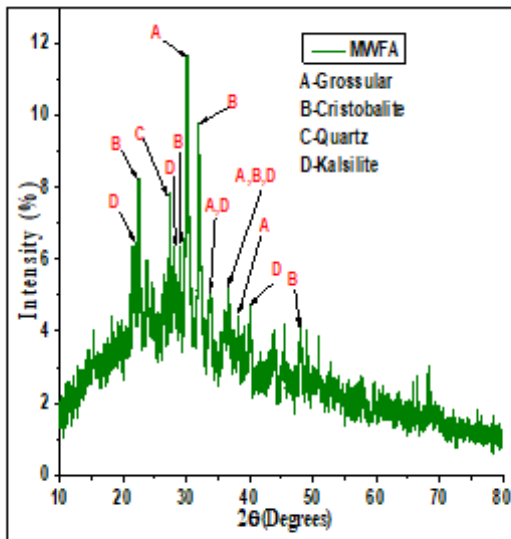
The diffractograms of the MWFA used for the synthesis are shown in Figure 4-6. Sharp peaks (labelled in alphabetical letters) indicate a crystalline phase while a hump (appearing at  $10 \leq 2\theta \leq 40$ ) shows the presence of an amorphous phase.

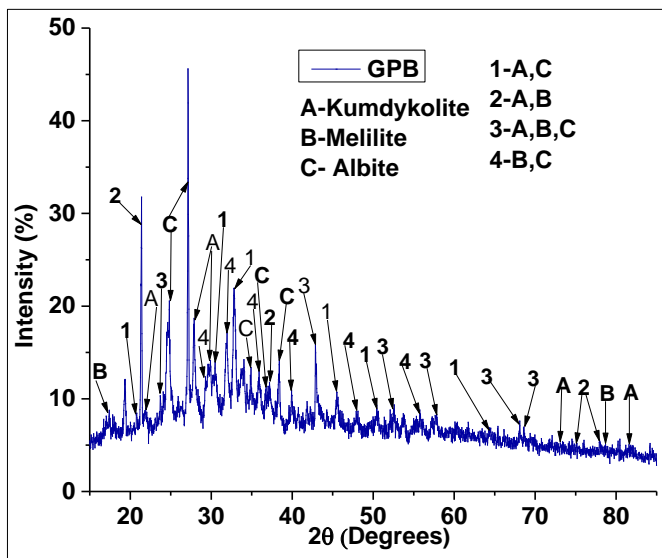
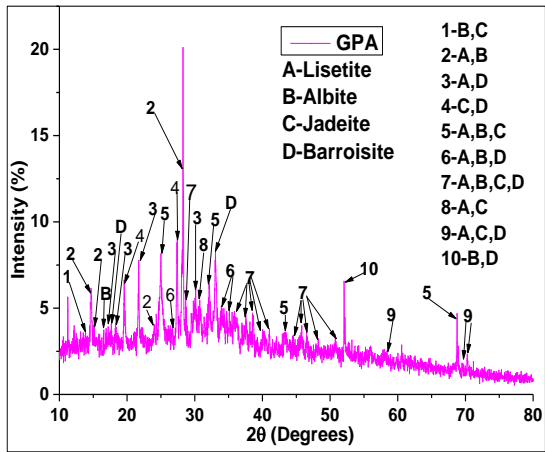
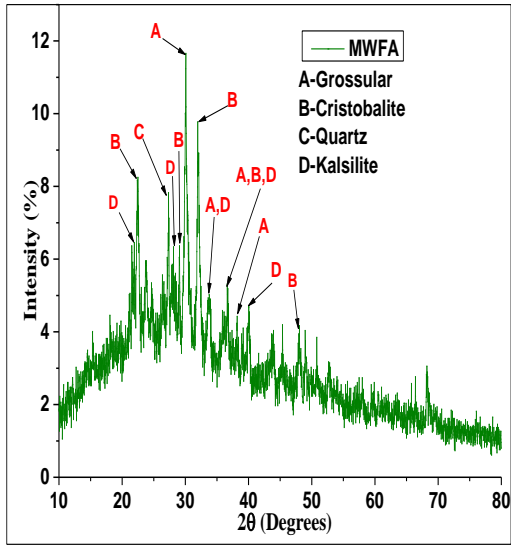
The MWFA had a degree of crystallinity (DOC) of 17.40% and the amorphous content was 82.60% by weight. The following four crystalline phases were identified in MWFA; 37.3% grossular ( $\text{Al}_2\text{Ca}_3\text{O}_{12}\text{Si}_3$ ) (cubic crystal system) [PDF# 96-900-0442], 34.4% cristobalite ( $\text{SiO}_2$ ) (tetragonal) [PDF# 96-900-1581], 21.2% quartz ( $\text{SiO}_2$ ) (trigonal-hexagonal axes) [PDF# 96-901-1495], 7.2% kalsilite ( $\text{AlKO}_4\text{Si}$ ) (hexagonal) [PDF# 96-900-9729]. The unidentified peak area was 13.3%.



**Figure 4.6: XRD diffractograms for MWFA**

The diffractograms of the three studied geopolymers GPA, GPB, GPC, and aluminosilicate source (MWFA) used for the synthesis are shown in Figure 4-7. The crystalline phases, degree of crystallinity (DOC), and amorphous contents were determined using Rietveld Method on Match XRD software. The DOC was calculated by dividing the total area of the crystalline peaks by the total area under the diffraction curve. On the other hand, the amorphous content was calculated by dividing the total area of amorphous peaks by the total area under the diffraction curve. The raw data of the diffraction patterns were analyzed using Match XRD software. For a selected phase, the total area of matched peak divided by the total area of the crystalline phase peaks gave the phase quantification.





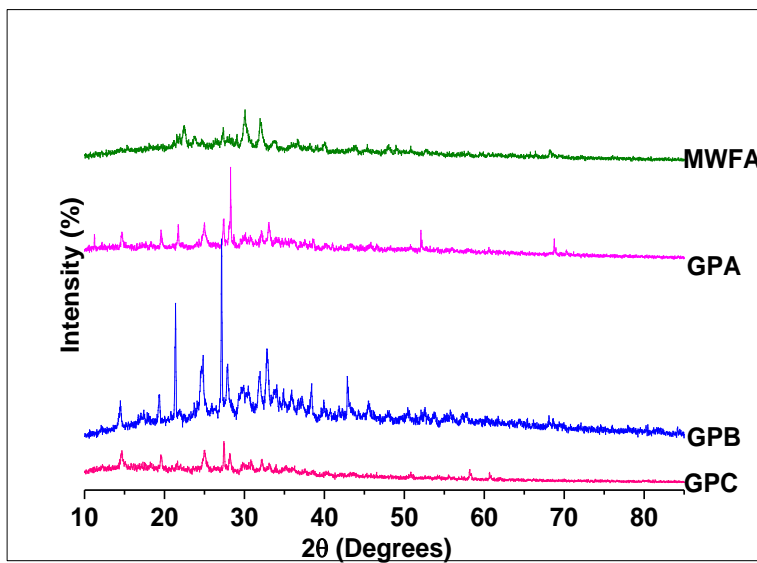
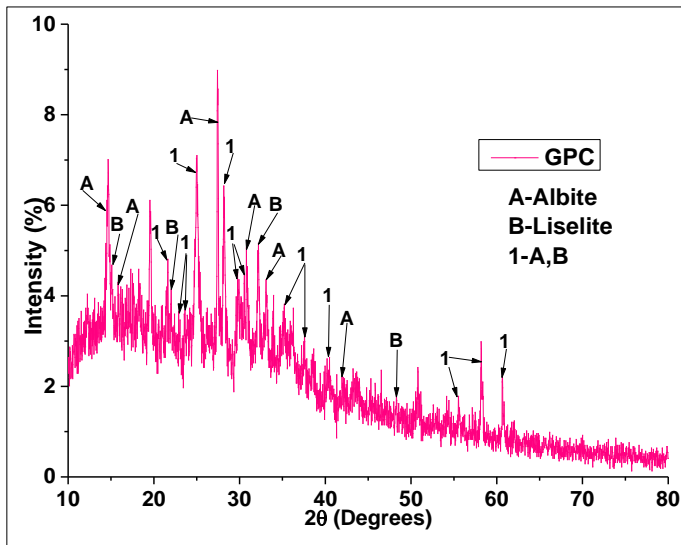


**Figure 4.7: XRD diffractograms for MWFA, GPA, GPB, and GPC**

The MWFA had a DOC of 17.40% and the amorphous content was 82.60% by weight. The following four crystalline phases were identified in MWFA; 37.3% grossular ( $\text{Al}_2\text{Ca}_3\text{O}_{12}\text{Si}_3$ ) (cubic crystal system) [PDF# 96-900-0442], 34.4% cristobalite ( $\text{SiO}_2$ ) (tetragonal) [PDF# 96-900-1581], 21.2% quartz ( $\text{SiO}_2$ ) (trigonal-hexagonal axes) [PDF# 96-901-1495], 7.2% kalsilite ( $\text{AlKO}_4\text{Si}$ ) (hexagonal) [PDF# 96-900-9729]. The unidentified peak area was 13.3%. The GPA had a DOC of 20.45% and the amorphous content was 79.55% by weight. The following four crystalline phases were identified in GPA; 47.3% liselite

$(\text{Al}_{3.96}\text{Ca}_{0.98}\text{Na}_{1.97}\text{O}_{16}\text{Si}_{4.04})$  (orthorhombic) [PDF# 96-900-1030], 23.2% Albite ( $\text{AlNaO}_8\text{Si}_3$ ) (triclinic (anorthic)), [PDF# 96-900-3701], 19.3% Jadeite ( $\text{AlNaO}_6\text{Si}_2$ ) (monoclinic) [PDF# 96-900-0344], 10.1% barroisite ( $\text{Al}_2\text{CaH}_2\text{Mg}_3\text{NaO}_{24}\text{Si}_8$ ) (monoclinic) [PDF# 96-901-6521]. The unidentified peak area was 15.0%.

The GPB had a DOC of 14.88% and the amorphous content was 85.12% by weight. The following three crystalline phases were identified in GPB; 52.4% kumdykolite ( $\text{AlNaO}_8\text{Si}_3$ ) (orthorhombic), [PDF# 96-154-4371], 25.1% melilite ( $\text{AlCaNaO}_7\text{Si}_2$ ) (tetragonal), [96-900-8196], 22.5% albite ( $\text{AlNaO}_8\text{Si}_3$ ) (triclinic (anorthic)), [PDF# 96-900-3702]. The unidentified peak area was 11.4%.

The GPC had a DOC of 21.26% and the amorphous content was 78.74% by weight. The following two crystalline phases were identified in GPC; 53.2% Albite ( $\text{AlNaO}_8\text{Si}_3$ ) (triclinic (anorthic)), [PDF# 96-900-0586], and 46.8% lisetite ( $\text{Al}_{3.96}\text{Ca}_{0.98}\text{Na}_{1.97}\text{O}_{16}\text{Si}_{4.04}$ ) (orthorhombic), [PDF# 96-900-1030]. The unidentified peak area was 17.4%. The changes in sodium silicate to sodium hydroxide mole ratios favoured the formation of new mineral phases resulting in geopolymers with varied chemical compositions (El Alouani *et al.*, 2018). Ibrahim *et al.* (2022) reported similar diffractograms in which quartz ( $\text{SiO}_2$ ) emerged as a major crystalline peak at  $2\theta$  values of  $27.993^\circ$  and less intense peaks at  $20.836^\circ$ ,  $40.479^\circ$ ,  $44.484^\circ$ ,  $50.535^\circ$  and  $67.42^\circ$  in the fly ash and the synthesized geopolymer. The study also reported similar phases such as mullite.

#### 4.2.4 Point of Zero Charge (pHpzc) Studies

The  $\text{pH}_{\text{pzc}}$  for MWFA was found to be at pH 8.1 as shown in Figure 4-8. The surface of MWFA became positively charged below pH 8.1, neutral at pH 8.1, and negatively charged above pH 8.1.

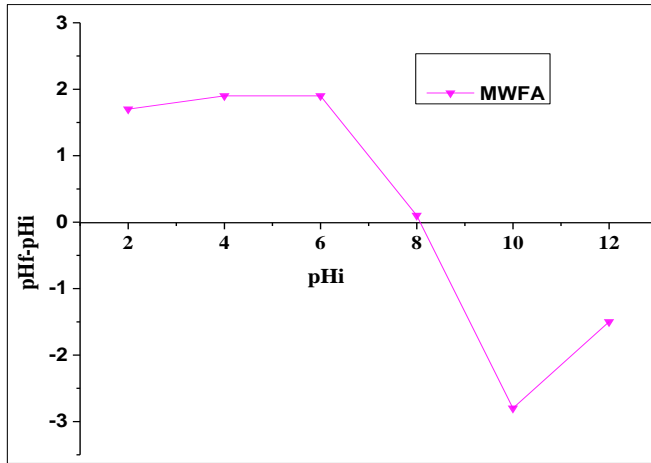


**Figure 4.8: The pH point of zero charge of MWFA**

Designing adsorption-based separation techniques between a solid and liquid phase depends on the surface chemistry of the adsorbent described by its point of zero charge ( $\text{pH}_{\text{pzc}}$ ). The  $\text{pH}_{\text{pzc}}$  is the average pH value of the adsorbent in the NaCl electrolyte. The  $\text{pH}_{\text{pzc}}$  was found to be at pH 8.1, 6.8, 6.7, and 6.8 for MWFA, GPA, GPB, and GPC, respectively (Figure 4-9) showing that geopolymerization affected the surface properties. For instance, GPB became positively charged below pH 6.7, neutral at pH 6.7, and negatively charged above pH 6.7. The  $\text{pH}_{\text{pzc}}$  is observed to be independent of the sodium silicate to sodium hydroxide mole ratios of the alkaline activator solution. Values comparable to those in this study and similar findings have been reported by Hermann *et al.* (2022); Sarkar *et al.* (2019).

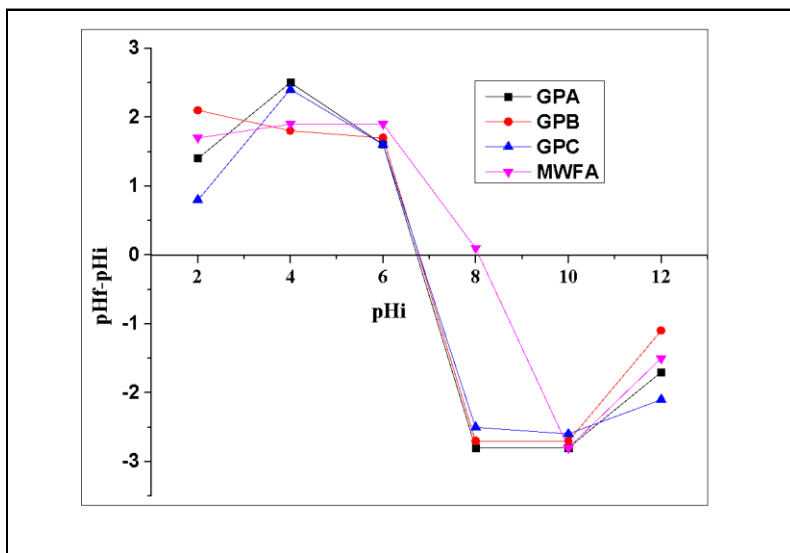


**Figure 4.9: The pH point of zero charge of MWFA, GPA, GPB, and GPC**

### 4.3 Adsorption Experiments

#### 4.3.1 Calibration Curves

In order to obtain the residual endosulfan concentrations, the calibration curves obtained in the concentration range 0 – 20 mg/L afforded a linear regression coefficient,  $R^2 > 0.99$  as shown in Figure 4-10. The linearity confirmed reliable quantitative analysis. The linear equation is shown below:

$$y = 0.0087x - 0.0011$$

4-1

The control experiment showed that undetectable amount of the endosulfan were adsorbed on the glass container walls. The pH of endosulfan solution following treatment with MWFA was constant in the range of pH 5.0 -5.2.

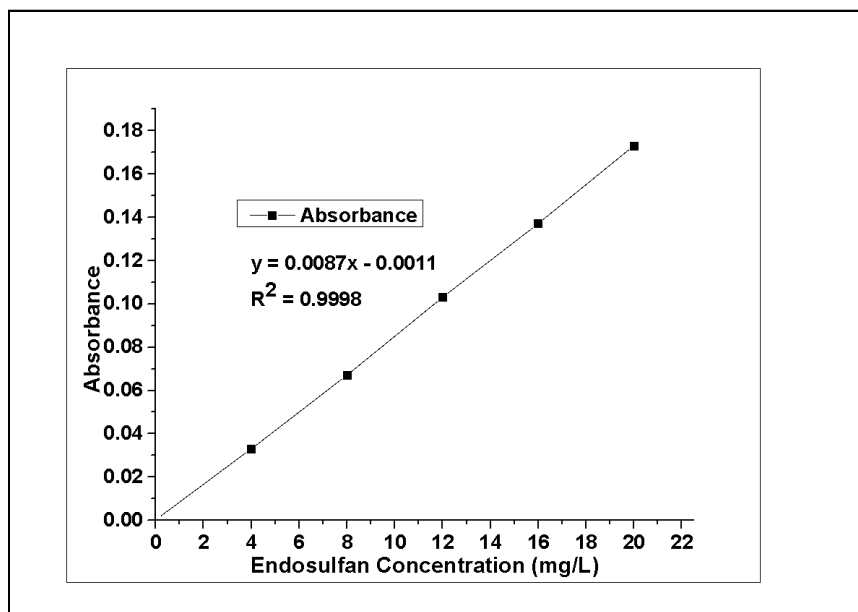


**Figure 4.10: Calibration curve for endosulfan**

#### 4.3.2 Effect of pH on Adsorption Mechanism

At lower pH conditions below  $pH_{pzc}$  6.8, the Si-OH and Al-OH centres of the geopolymer were protonated due to a high concentration of  $H^+$  ions (Figure 4.11). As a result, the adsorbent surface became positively charged ( $GP^+$ ) and the negatively charged endosulfan moieties ( $pK_a = -5.5$ ) are electrostatically attracted to the geopolymer surface. This results in increased adsorption at low pH (Figure 4-12). Similar phenomenon was observed for adsorption of alpha and beta endosulfan onto bentonite clay (Rauf *et al.*, 2012) and uptake of endosulfan by saw dust derived activated carbon (Kakoi *et al.*, 2015).

At higher pH, the Si-OH and Al-OH groups in the geopolymer were deprotonated hence the geopolymer surface became negatively charged. Consequently, coulombic repulsion forces

between the adsorbent surface and anionic adsorbate ions became significant resulting in decreased adsorption. Similar sequence was reported for the removal of anionic eriochrome black T dye onto alkali activated volcanic ash based geopolymer (Tome *et al.*, 2021). The decrease in adsorption at high pH is also attributed to competition between the hydroxide ions ( $\text{OH}^-$ ) and negatively charged endosulfan for the same adsorption sites. Besides electrostatic interactions, hydrogen bonding between the hydrogen in the hydroxyl ( $-\text{OH}$ ) groups on the adsorbent surface and the lone pairs of electrons of the electronegative O and Cl atoms of endosulfan is proposed. This is consistent with reports by Owino *et al.* (2023) for the removal of anionic dye, bromocresol green, using solid waste fly ash based geopolymers. Very low pH ranges were unsuitable for practical application (Ikowska *et al.*, 2009). The optimum pH was found to be 5.0 as shown in Figure 4-12. Further details on adsorption mechanism is discussed under kinetics, isotherms and thermodynamic studies.

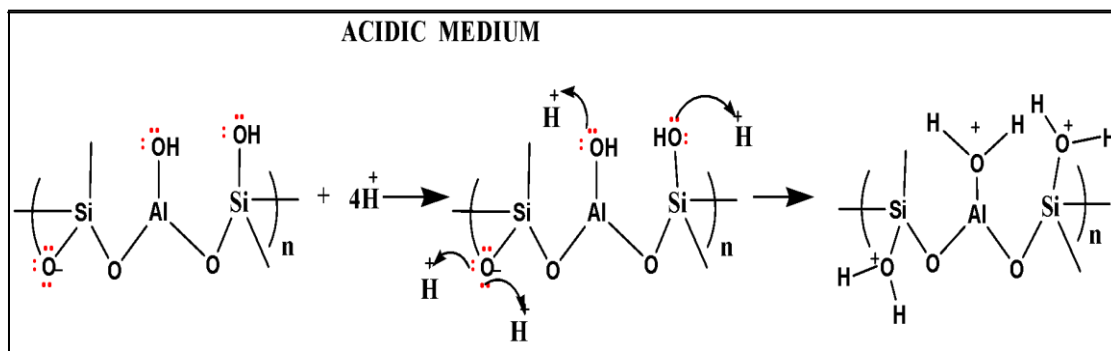


**Figure 4.11: Surface charge of the MWFA-based geopolymer in acidic medium**

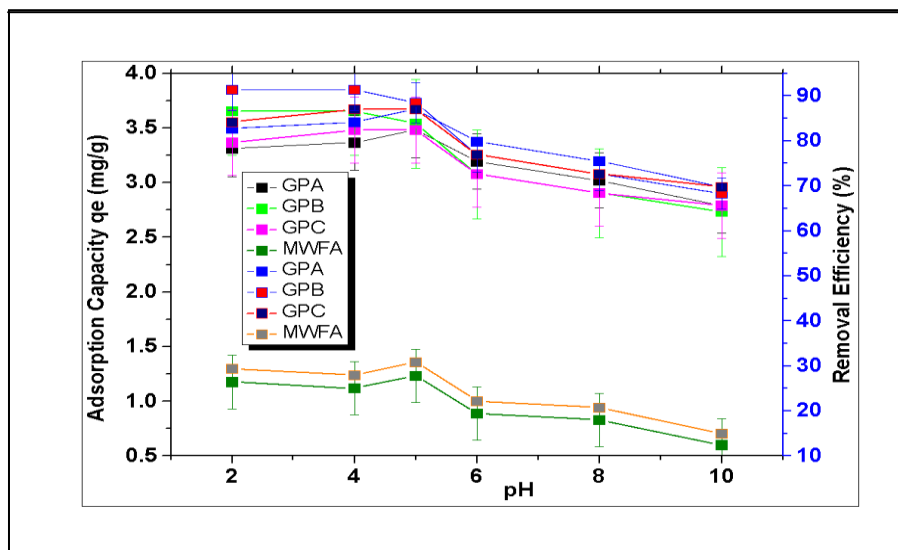


**Figure 4.12: Graph of adsorption capacity and removal efficiency against pH**



### 4.3.3 Effect of Initial Concentration

The adsorption capacity was found to increase with an increase in initial concentration of the endosulfan (Figure 4-13). This phenomenon can be explained by the fact that at low concentrations, the majority of the adsorption sites remained unoccupied due to low adsorbate / adsorbent interactions leading to low adsorption capacity. However, when the initial concentration of endosulfan was increased, it resulted to increased adsorbate/adsorbent interactions and mass gradient between the solid phase and the bulk solution until the maximum adsorption capacity was reached. Similar trend was reported for the adsorption of methylene blue dye by geopolymers derived from common clay and rice husk ash (Maingi *et al.*, 2017) and volcanic ash-metakaolin based geopolymers (Shikuku *et al.*, 2022).

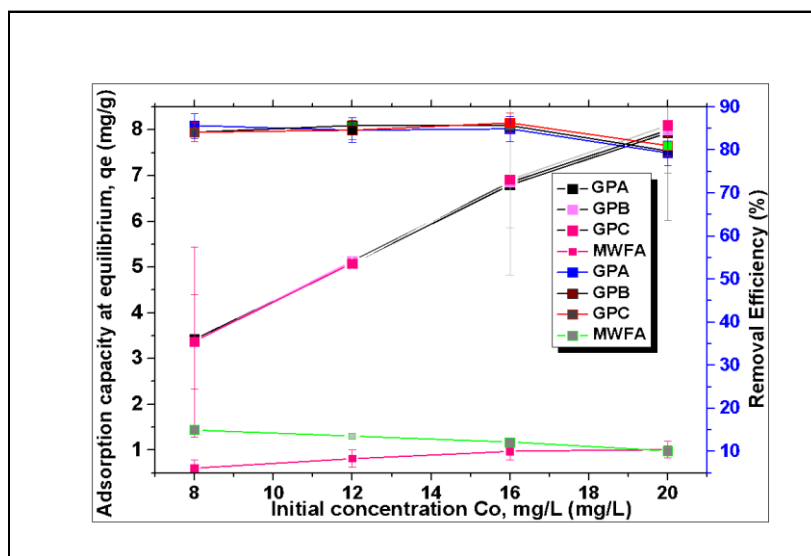


**Figure 4.13: Variation of adsorption capacity and removal efficiency with initial concentration**

### 4.3.4 Effect of Contact Time

The time-dependent evolution of the geopolymer sorption capacity for endosulfan depicted fast sorption kinetics leading to saturation within 90 min (Figure 4-14) followed by an equilibrium phase. Noteworthy, the geopolymers exhibited higher removal efficiencies for endosulfan (> 83 %) than MWFA (20.58 %) as shown in Table 4-3. Geopolymerization improved the removal efficiency of the raw material by approximately 4-orders of magnitude. Tome *et al.* (2023) also noted that geopolymerization increased the adsorption capacity by 5-orders of magnitude for laterite-based geopolymers. Geopolymerization is therefore demonstrated to be a beneficial step.

**Table 4.3: Variation of adsorption capacity, at, (mg/g) with time (minutes) ( $C_o = 8$  mg/L,  $T = 303$  K)**

Time (Minutes)	Adsorption Capacity, qt, (mg/g)			
	GPA	GPB	GPC	MWFA
0	0.13825	0.13825	0.13825	0.02297
10	1.00282	1.29101	1.17573	0.31116
20	1.34865	1.46392	1.5792	0.42644
30	1.86739	1.80975	2.0403	0.48408
40	2.09794	2.09794	2.44377	0.77227
50	2.44377	2.50141	2.61669	0.88754
60	2.90488	2.96251	2.7896	1.00282
90	3.30834	3.30834	3.42362	1.06046
120	3.42362	3.42362	3.48126	1.23337
150	3.5389	3.5389	3.65417	1.34865

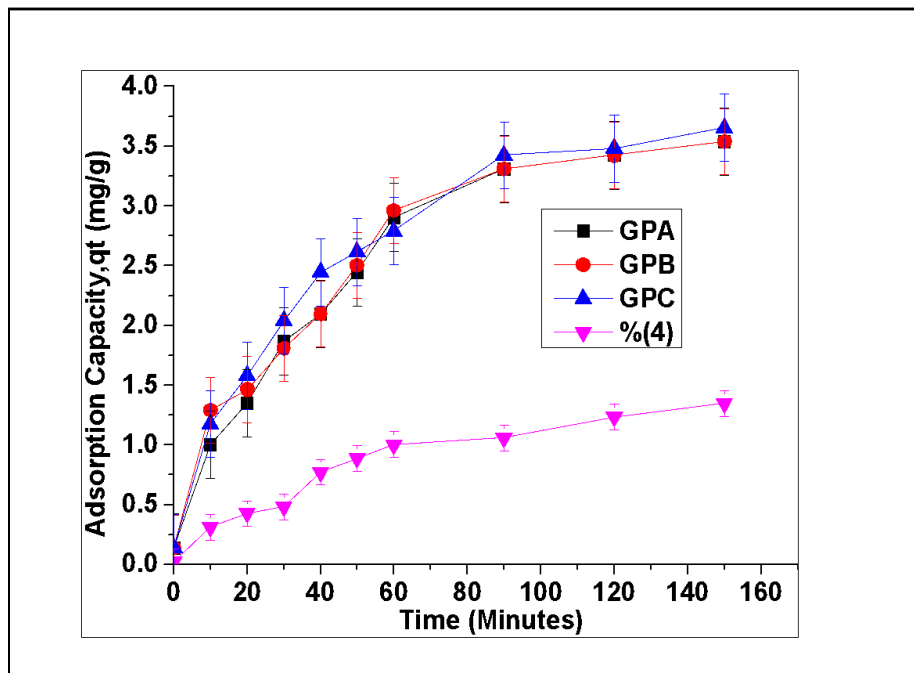


**Figure 4.14: Evolution of sorption capacity of GPA, GPB, GPC, and MWFA for endosulfan with time ( $m = 0.1$ g/50mL,  $C_i = 8$ mg/L,  $pH = 5$ )**

#### 4.3.5 Kinetics Studies

The adsorption kinetics for endosulfan onto the geopolymers were analyzed using Lagergren *pseudo*-first-order (PFO) and *pseudo*-second-order (PSO) kinetic models.

**Table 4.4: Lagergren pseudo-first-order (PFO) and Pseudo-second-order (PSO) parameters**

Model	Parameter	GPA	GPB	GPC	MWFA
PFO	$K_1$ ( $\text{min}^{-1}$ )	0.024	0.026	0.028	0.019
	$q_e$ (cal) ( $\text{mg g}^{-1}$ )	3.661	3.604	3.635	1.399
	$q_e$ (exp) ( $\text{mg g}^{-1}$ )	3.308	3.308	3.424	1.061
	S rate ( $\text{mg.g}^{-1}.\text{min}^{-1}$ )	0.088	0.093	0.102	0.027
	$t^{1/2}$ (min)	28.88	26.66	24.76	36.48
	$R^2$	0.978	0.974	0.996	0.955
PSO	$K_2$ ( $\text{g mg}^{-1} \text{min}^{-1}$ )	0.027	0.027	0.028	0.009
	$q_e$ (cal) ( $\text{mg g}^{-1}$ )	0.689	0.690	0.691	0.688
	$q_e$ (exp) ( $\text{mg g}^{-1}$ )	3.308	3.308	3.424	1.061
	S rate ( $\text{mg.g}^{-1}.\text{min}^{-1}$ )	0.128	0.129	0.134	0.004
	$t^{1/2}$ (min)	53.75	53.68	51.68	161.5
	$R^2$	0.875	0.880	0.895	0.847

Coefficients of determination ( $R^2$ ) values have been used extensively as the criterion for discriminating best-fitting models (Dzoujo *et al.*, 2022; Tome *et al.*, 2022; Tome *et al.*, 2023; Shikuku *et al.*, 2022). From Table 4-4, since the coefficients of determination ( $R^2$ ) values for the PFO were closer to unity than PSO, the adsorption kinetics were best accounted for and predicted by the PFO kinetic model. The initial adsorption rates ( $S_{\text{rate}}$ ) decreased in the order  $0.102 > 0.093 > 0.088 > 0.027$  for GPC, GPB, GPA, and MWFA, respectively, with a decrease in sodium silicate to sodium hydroxide mole ratios. Relative to the precursor, MWFA, the adsorption rate ( $k_1$ ) was ~1.5 times higher for the geopolymers, an indication that geopolymerization enhanced the number and accessibility to the adsorption sites.

Similarly, geopolymerization increased the adsorption rate by 3-8 orders of magnitude for the removal of methylene blue dye onto volcanic ash-metakaolin based geopolymers relative to the precursors (Shikuku *et al.*, 2022). However, the adsorption of methylene blue was described by the PSO model. The rate constant ( $k_1$ ) showed minute variation across the geopolymer adsorbents. The adsorption rate ( $k_1$ ) was therefore weakly influenced by the chemical composition of the materials. This is contrary to results by Shikuku *et al.* (2022)

where rate constant was dependent on geopolymer composition. This illustrates that functional group density and accessibility vary with synthesis conditions.

At the onset, when all adsorption sites are vacant, the GPC had the highest initial adsorption rate ( $S_{\text{rate}}$ ) indicating that it had the highest number of energetically favourable and accessible adsorption sites thus controlling the adsorption half-life ( $t_{1/2}$ ). The sodium silicate to sodium hydroxide mole ratio of the activator solution had a bearing on the accessibility of the favoured adsorption sites. Conformity to PFO suggests a physisorption-mediated rate-determining step (Revellame *et al.*, 2020; Gupta *et al.*, 2021; El Alouani *et al.*, 2018).

#### **4.3.6 Thermodynamics of Endosulfan Adsorption**

Temperature rise led to an increase in the amount of endosulfan adsorbed indicating an endothermic reaction. As the temperature increased, the kinetic energy of endosulfan molecules increased leading to an increase in mobility of the adsorbate molecules and the number of interactions with active sites. An increase in temperature also decreased the boundary layer and this led to an increase in adsorption. Similar phenomenon was used to account for the endothermic adsorption of methylene blue dye onto pozzolan-biochar geopolymer composites (Dzoujo *et al.*, 2022).

The effect of temperature changes on the sorption was studied in the range 303-353 K. The thermodynamic parameters, namely, change in Gibbs free energy ( $\Delta G$ ), enthalpy ( $\Delta H$ ), and entropy ( $\Delta S$ ), which indicate the practical feasibility of the process, post-adsorption structural changes of the adsorbent and the adsorption mechanism, were derived using the van't Hoff plot (Figure 4-15).

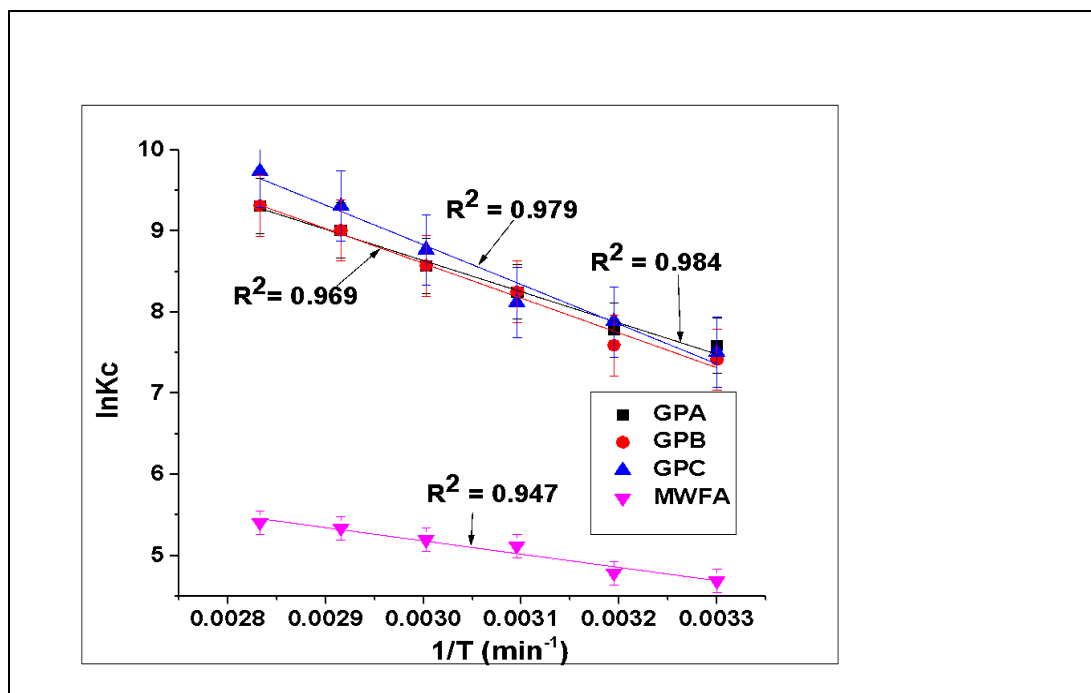


**Figure 4.15: The Van't Hoff plots for MWFA, GPA, GPB and GPC**

The positive  $\Delta H^{\circ}_{\text{ads}}$  (kJ/mol) values for all the geopolymers confirmed an endothermic process. According to Jemutai-Kimosop *et al.* (2022),  $\Delta H$  values above 40 kJ/mol corresponds to chemisorption mechanisms. In this study, all the enthalpy values were very low ( $\leq 40$  kJ/mol) which corresponds to physisorption processes. Similar results were reported for the adsorption of endosulfan onto amine-modified magnetic diatomite, an aluminosilicate based adsorbent (Alacabey *et al.*, 2022).

The positive  $\Delta S^{\circ}_{\text{ads}}$  (J/K) value indicated that, at the liquid-solid interface, there was an increased disorderliness (Shikuku *et al.*, 2018).

The negative  $\Delta G^{\circ}_{\text{ads}}$  (kJ/mol) values (Table 4-5) indicated that the adsorption processes were spontaneous and favourable. The relatively low magnitudes of  $\Delta G^{\circ}_{\text{ads}}$  values supported the aforementioned physical adsorption mechanism (Dzoujo *et al.*, 2022; Hermann *et al.*, 2022). The thermodynamics data showed that the adsorption of endosulfan by the MWFA- based geopolymers was an entropy-driven process.

**Table 4.5: Thermodynamic parameters of GPA, GPB, GPC, and MWFA**

T (K)	GPA			GPB			GPC			MWFA		
	$\Delta H^*$ ads kJ/mol	$\Delta G^*$ ads kJ/mol	$\Delta S^*$ ads J/K/mol	$\Delta H^*$ ads kJ/mol	$\Delta G^*$ ads kJ/mol	$\Delta S^*$ ads J/K/mol	$\Delta H^*$ ads kJ/mol	$\Delta G^*$ ads kJ/mol	$\Delta S^*$ ads J/K/mol	$\Delta H^*$ ads kJ/mol	$\Delta G^*$ ads kJ/mol	$\Delta S^*$ ads J/K/mol
303	31.98	-18.85	167.75	35.65	-18.69	178.48	40.67	-18.90	195.44	13.61	-11.81	83.91
313		-20.26			-19.75			-20.52			-12.45	
323		-22.16			-22.16			-21.80			-13.75	
333		-23.73			-23.73			-24.28			-14.38	
343		-25.69			-25.69			-26.55			-15.22	
353		-27.33			-27.33			-28.56			-15.87	
E <sub>a</sub> kJ/mol	28.57			31.49			36.78			3.25		
S <sup>*</sup>	$2.6676 \times 10^{-6}$			$9.5622 \times 10^{-7}$			$1.1482 \times 10^{-7}$			$2.2630 \times 10^{-1}$		

The sticking probability,  $S^*$ , and adsorption activation energy ( $E_a$ ) were computed from experimental data using the modified Arrhenius-type equation (equation 4-10) related to surface coverage ( $\theta$ ) (Shikuku *et al.*, 2018) and plotted as shown in Figure 4-16.

$$\ln(1 - \theta) = \ln S^* + \frac{E_a}{R} \quad 4-10$$

The value of  $\theta$  was determined using equation 4-11:

$$\theta = \left[ 1 - \frac{C_e}{C_i} \right] \quad 4-11$$

Where  $C_e$  is the equilibrium endosulfan concentration (mg/L),  $C_i$  is the initial endosulfan concentration (mg/L) and R is the universal gas constant (8.314 J/K.mol).

The sodium silicate to sodium hydroxide mole ratio had a bearing on activation energies. Activation energies for the adsorption processes were found to be 28.57, 31.49, 36.78, and 3.25 kJ/mol for GPA, GPB, GPC, and MWFA, respectively indicating that there was purely physisorption due to minimal electrostatic interaction between MWFA and endosulfan. The  $E_a$  values and  $\Delta H^{\circ}_{ads}$  values were all lower than 40 kJ/mol and this consistency confirmed majorly physical adsorption processes.

The  $S^*$  depends on the adsorbate/adsorbent system under study and temperature.  $S^*$  value lies in the range  $0 < S^* < 1$ . The  $S^*$  values were found to be  $2.6676 \times 10^{-6}$ ,  $9.5622 \times 10^{-7}$ ,  $1.1482 \times 10^{-7}$ , and  $2.2630 \times 10^{-1}$  for GPA, GPB, GPC, and MWFA, respectively. The sticking probability ( $S^*$ ) was found to be very low indicating a low probability for the endosulfan molecules to stick on the adsorbent surface upon collision, a testament to a physisorption mechanism with almost no exchange of electrons (Shikuku *et al.*, 2018).

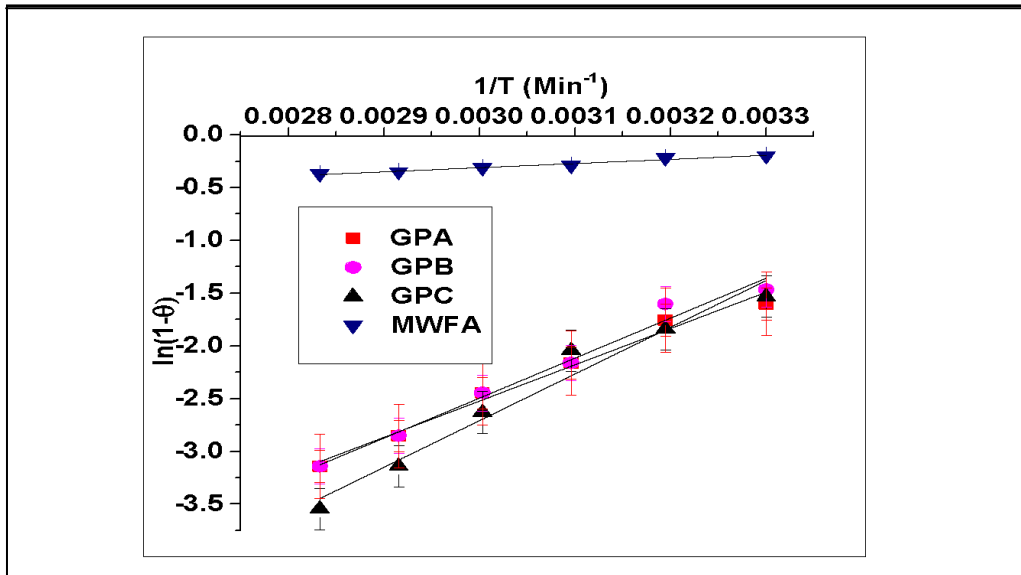


Figure 4.16: Arrhenius-type equation plots for MWFA, GPA, GPB and GPC

#### 4.3.8 Adsorption Isotherms

Equation 4-12 describes the nonlinear Langmuir isotherm (Langmuir 1918):

$$q_e = \frac{Q_0 K_L C_e}{1 + K_L C_e} \quad 4-12$$

$C_e$  represents the equilibrium concentration of endosulfan adsorbate (mg/L) while  $q_e$  is the amount of endosulfan adsorbed at equilibrium (mg/g). The  $Q_0$  represents the monolayer maximum adsorption capacity (mg/g), and the Langmuir adsorption constant,  $K_L$  (L/mg), is related to the free energy of adsorption.

According to the Langmuir isotherm model, there occurred single-layer adsorption of adsorbate molecules onto a fixed number of active sites and there was no lateral interaction between adsorbed molecules on a morphologically homogeneous surface. The adsorption sites were, in this case, considered to be identical (Peydayesh *et al.*, 2014; Karaer and Kaya, 2016; Zulkifly *et al.*, 2019).

Equation 4-13 describes the Langmuir isotherm expressed using a dimensionless parameter called the separation factor ( $R_L$ ), as follows:

$$R_L = \frac{1}{1 + K_L C_i}$$

4-13

$R_L$  values indicate the nature and feasibility of the isotherm as favourable ( $0 < R_L < 1$ ), unfavourable ( $R_L > 1$ ), linear ( $R_L = 1$ ), and irreversible ( $R_L = 0$ ) (Ofomaja, 2008). Equation 4-14 expresses Freundlich isotherm:

$$q_e = K_F C_e^{1/n}$$

4-14

Where  $q_e$  (mg/g), is the adsorbed amount of adsorbate at equilibrium. Freundlich constant  $K_F$ , ((mg/g) × (L/mg)<sup>1/n</sup>) indicates the relative adsorption capacity of the adsorbent (mg /g); ‘n’ is the Freundlich exponent and 1/n is the Freundlich intensity parameter, a constant that shows the intensity of the adsorption. The  $C_e$  (mg /L) value was the equilibrium concentration of adsorbate.

The Freundlich equation has two constant  $K_L$  and 1/n for a given adsorbent and adsorbate respectively at a particular temperature. High  $K_F$  and low values of 1/n indicate high adsorption throughout the concentration range studied whereas high values of 1/n and low  $K_F$  values indicate low adsorption (Treybal, 1980). Freundlich intensity parameter also shows surface heterogeneity where it becomes more heterogeneous as its value gets closer to zero.

Freundlich equation is exponential; therefore, the amount of adsorbate on the adsorbent surfaces rises with an increase in solute concentration. Using equation 4-15, Halsey determined what is known as Freundlich maximum adsorption capacity (Halsey, 1948):

$$q_m = K_F C_i^{1/n}$$

4-15

where  $C_i$  is the initial solute concentration (mg/L) and  $q_m$  is the Freundlich maximum adsorption capacity (mg/g).

The equilibrium data were tested against the two classical nonlinear adsorption models. The nonlinear regression was performed by minimization of the values of the regression sum of squares (RSS) expressed as equation 4-16 (Shikuku *et al.*, 2018):

$$RSS = \sum_1^N (q_{e,experimental} - q_{e,predicted})^2$$

4-16

The best-fitting model was determined using the coefficient of determination ( $R^2$ ) values. The relatively high coefficient of determination ( $R^2$ ) values (Table 4-6) indicate that the adsorption of endosulfan onto the geopolymers was best predicted by the Langmuir isotherm. The  $R_L$  values were between 0 and 1 for all the adsorbents indicating that the adsorption



processes are favourable (Meroufel *et al.*, 2013). The adsorption of endosulfan onto an aluminosilicate based adsorbent, amine-modified magnetic diatomite, was similarly described by the Langmuir isotherm (Alacabey *et al.*, 2022). Similar observation was reported for the removal of endosulfan onto wood charcoal (Yedla and Dikshit, 2008).

**Table 4.6: Langmuir and Freundlich isotherm models parameters**

	Langmuir isotherm model					Freundlich isotherm model				
	Q <sub>o</sub> (mg/g)	K <sub>L</sub> (L/ mol)	K <sub>a</sub>	RL	R <sup>2</sup>	R <sup>2</sup>	K <sub>F</sub> (mg /g)	q <sub>m</sub> (mg /g)	$\frac{1}{n}$	n
GPA	15.899	0.258	4.10	0.162	0.971	0.943	3.288	23.676	0.659	1.517
GPB	16.970	0.238	4.04	0.174	0.951	0.921	3.301	25.162	0.678	1.475
GPC	20.010	0.191	3.82	0.207	0.944	0.923	3.229	28.848	0.731	1.368
MWFA	1.872	0.070	0.13	0.417	0.987	0.964	0.184	1.141	0.609	1.642

The monolayer maximum adsorption capacities (Q<sub>o</sub>) were 15.89, 16.97, 20.01, and 1.87 mg/g for GPA, GPB, GPC, and MWFA respectively. Notably, the adsorption capacities of the geopolymers were substantially higher (~8-10 times) than that of MWFA attesting that geopolymerization was a beneficial step. Additionally, the adsorption capacity of the geopolymers increased with increasing sodium silicate to sodium hydroxide ratios. The apparent equilibrium constant (K<sub>a</sub>), a product of Q<sub>o</sub> and K<sub>L</sub>, derived from the Langmuir isotherm, is a measure of the relative affinity of the adsorbent towards the endosulfan molecules (Mishra and Tiwari, 2006). The apparent equilibrium constant values (Table 4-6) indicates that the affinity of the geopolymers for endosulfan is much higher (~30 times) than that of MWFA indicating that geopolymerization process imparts surface properties such as lower pH<sub>pzc</sub> and higher porosity which enables the geopolymers to have higher affinity for endosulfan.

Additionally, the geopolymers had a similar affinity toward endosulfan. This shows that the difference in chemical compositions of the geopolymers, from the XRD data, could not account for the trends in their adsorption capacities. This is further supported by the FTIR data that showed no new functional groups that would induce increased affinity. The increase in adsorption capacity with an increase in sodium silicate to sodium hydroxide mole ratios is attributed to increased accessibility to the energetically favoured binding sites. The adsorption capacity of geopolymers is therefore neither necessarily nor solely controlled by

their composition. A trade-off between composition and textural properties is inferred (Tome *et al.*, 2023).

On the other hand, the Freundlich model (Freundlich, 1906) proposes multilayer adsorption. This kind of adsorption has differing dispersion of adsorption affinities onto the heterogeneous surface of the adsorbent without lateral interaction. In line with this postulate, the adsorption sites which were energetically favoured were occupied first, followed by that had diminishing binding energies with increasing rates of site occupancy.

The  $K_F$  and  $1/n$  for the geopolymers were higher than the MWFA indicating that geopolymerization improved the affinity for the endosulfan. However, the  $K_F$  values for the geopolymers were invariable (Table 4-6) indicating that the affinity of the geopolymers for endosulfan was independent of the composition. This is consistent with the apparent equilibrium constants ( $K_a$ ) from the Langmuir isotherm. The Freundlich factor ( $1/n$ ) values less than unity correspond to heterogeneous adsorbent surfaces. Additionally, the magnitudes of  $1/n$  suggest weak adsorbent-adsorbate interactions corresponding to the physisorption mechanism (Shikuku and Jemutai-Kimosop, 2020). This is supported by the thermodynamics data.

The adsorption capacities of the geopolymers in this study were compared with those adsorbents reported in the literature for the removal of endosulfan from water (Table 4-7). It is observed that the adsorption capacity of geopolymers, especially GPC, was higher than most of the adsorbents. MWFA-based geopolymers are therefore promising adsorbents for the sequestration of endosulfan from water.

**Table 4.7: A comparison of adsorption capacities of MWFA-based geopolymers with other adsorbents for endosulfan**

<b>Adsorbents</b>	<b>Q<sub>o</sub> (mg/g)</b>	<b>Reference</b>
GPA	15.899	This study
GPB	16.970	This study
GPC	20.010	This study
MWFA	1.872	This study
Wood Charcoal	0.530	Yedla and Dikshit (2008)
Amine-modified magnetic diatomite	97.200	Alacabey (2022)
Raw diatomite	16.600	Alacabey (2022)
Carbon Slurry	34.110	Gupta and Imran (2008)
Activated charcoal	2.145	Sudhakar and Dikshit (1999)
Wood charcoal	1.773	Sudhakar and Dikshit (1999)
<i>Sojar caju</i>	1.575	Sudhakar and Dikshit (1999)
kimberlite tailings	0.882	Sudhakar and Dikshit (1999)
Silica	0.323	Sudhakar and Dikshit (1999)

## CHAPTER FIVE

### CONCLUSIONS, RECOMMENDATIONS AND SUGGESTIONS FOR FURTHER RESEARCH

#### 5.1 Conclusions

- i. Three MWFA-based geopolymers GPA, GPB, and GPC were synthesized via alkaline activation with increasing sodium silicate to sodium hydroxide mole ratios ratios of 0.17, 0.21, and 0.24 for GPA, GPB, and GPC, respectively.
- ii. The geopolymerization reaction was evidenced by the shift in the Si–O–T (T=Si or Al) asymmetric stretching vibrations towards lower wavenumbers  $968\text{ cm}^{-1}$ ,  $965\text{ cm}^{-1}$ ,  $970\text{ cm}^{-1}$  for GPA, GPB, and GPC, respectively, in relation to the band at  $989\text{ cm}^{-1}$  in the MWFA (FTIR), the formation of new mineral phases (XRD) and distinguishable morphologies (SEM-EDX). The aluminosilicate composition of MWFA was sufficient for geopolymer development.
- iii. Adsorption performance decreased with increase in pH. The effect of pH showed adsorption mechanism was largely due to electrostatic interactions. Removal efficiency increased with increase in initial endosulfan concentration. The adsorption kinetics of endosulfan onto the geopolymers followed the *pseudo*-first-order kinetics attaining equilibrium in 90 min and Langmuir isotherm model gave the best description of the equilibrium data. Amount adsorbed increased with the rise in temperature and adsorbent dosage. Thermodynamically, the adsorption processes were endothermic ( $\Delta H > 0$ ), spontaneous ( $\Delta G < 0$ ), physical, and entropy-driven.
- iv. The Langmuir maximum adsorption capacities increased in the order 1.872, 15.899, 16.970, and 20.010 mg/g with increasing sodium silicate to sodium hydroxide mole ratios for MWFA, GPA (0.17), GPB (0.21), and GPC (0.24), respectively. The sodium silicate to sodium hydroxide ratio of 0.24 produced an MWFA-based geopolymer with the highest adsorption capacity and performance. Alkalinization of MWFA was shown to be a beneficial pre-treatment step both for adsorption capacity and adsorption rate. The adsorbent-adsorbate affinity and adsorption rates were independent of the composition of the geopolymer.

## **5.2 Recommendations**

- i. MWFA with sufficient aluminosilicate content should be used for geopolymer development with higher silicate to NaOH ratios for maximization of the adsorption capacities for endosulfan removal in large scale water treatment systems.
- ii. In order to predict the mechanism of endosulfan removal using MWFA-based geopolymers in water treatment systems, the determined kinetic, thermodynamic and adsorption isotherm parameters should be applied.

## **5.3 Suggestions for Further Research**

- i. Evaluation of suitable solvents for desorption of endosulfan from an exhausted geopolymer to evaluate the number of cycles the MWFA-based geopolymers may be reused.
- ii. Suitable low-cost silica sources as replacement for commercial sodium silicate for the development of geopolymer adsorbents.
- iii. Other synthesis conditions that may affect or improve geopolymer adsorptive properties, such as use of additives, should be investigated further.

## REFERENCES

- Abdullah, M. M. A., Kamarudin, H., Bnhussain, M., Khairul Nizar, I., Rafiza, A. R., and Zarina, Y. (2011). The Relationship of NaOH Molarity, Na<sub>2</sub>SiO<sub>3</sub>/NaOH Ratio, Fly Ash/Alkaline Activator Ratio, and Curing Temperature to the Strength of Fly Ash-Based Geopolymer. *Advanced Materials Research*, 328–330, 1475–1482.  
<https://doi.org/10.4028/www.scientific.net/amr.328-330.1475>
- Abdullah, M. M. A. B., Ming, L. Y., Yong, H. C., and Tahir, M. F. M. (2018). Clay-Based Materials in Geopolymer Technology. *Cement Based Materials*.  
<http://dx.doi.org/10.5772/intechopen.74438>.
- Alacabey, I. (2022). Endosulfan Elimination Using Amine-Modified Magnetic Diatomite as an Adsorbent. *Frontiers in Chemistry*. **10**:907302.  
<https://doi.org/10.3389/fchem.2022.907302>
- Alba, N., Gassó, S., Lacorte, T., and Baldasano, J.M. (1997). Characterization of municipal solid waste incineration residues from facilities with different air pollution control systems. *Journal of the Air & Waste Management Association*, **47**(11): 1170–1179.  
<https://doi.org/10.1080/10473289.1997.10464059>.
- Al-Ghouti, M.A., Khan, M., Nasser, M.S., Al Saad, K. and Ee Heng, O. (2020). Application of geopolymers synthesized from incinerated municipal solid waste ashes for the removal of cationic dye from water. *Plos One Journal*, **15** (11). e0239095.  
<https://doi.org/10.1371/journal.pone.0239095>.
- Al-Samarai, G. F., Mahdi, W. M. and Al-Hilali, B. M. (2018). Reducing environmental pollution by chemical herbicides using natural plant derivatives – allelopathy effect. *Annals of agricultural and environmental medicine: AAEM*, **25**(3), 449-452.  
<https://doi.org/10.26444/aaem/90888>.
- Bhatnagar, A. and Minocha, A. (2006) Conventional and Non-Conventional Adsorbents for Removal of Pollutants from Water. *Indian Journal of Chemical Technology*, **13**, 203-217. <https://www.researchgate.net/publication/267822355>.
- Cozmuta, L.M., Cozmuta, A.M., Peter, A., Nicula, C., Nsimba, E.B., and Tutu, H. (2012). The influence of pH on the adsorption of lead by Na-clinoptilolite: Kinetic and equilibrium studies. *Water SA*, 38(2). <https://doi.org/10.4314/wsa.v38i2.13>.
- Craig, I.P, Bundschuh, J. and Thorpe, D. (2015). Pesticides Sustainable Management Practice (SMP) Including Porous Biochar/ Geopolymer structures for Contaminated Water Remediation. *International Journal of GEOMATE*, **9** (2), 1523-1527.

- Crini, G., Lichtfouse, E. (2018). Wastewater Treatment: An Overview. In: Crini, G., Lichtfouse, E. (eds) Green Adsorbents for Pollutant Removal. *Environmental Chemistry for a Sustainable World*, **18**, 1-22. [https://doi.org/10.1007/978-3-319-92111-2\\_1](https://doi.org/10.1007/978-3-319-92111-2_1).
- Daud, N. A. A., Shamsuddin, M. R., Pradanawati, S.A. and Rabat, N. E. (2021). Preparation, characterization and performance evaluation of fly ash-based composite geopolymer membranes for methylene blue dye removal. *Science, Engineering and Health Studies*, **15**, 21020011. <https://doi.org/10.14456/sehs.2021.38>.
- Davidovits, J. (1991) Geopolymers. *Journal of Thermal Analysis* **37**, 1633–1656. <https://doi.org/10.1007/BF01912193>
- Dewan, A., Bhatnagar, V. K., Mathur, M. L., Chakma, T., Kashyap, R., Sadhu, H. G., Sinha, S. N., & Saiyed, H. N. (2004). Repeated episodes of endosulfan poisoning. *Journal of toxicology. Clinical toxicology*, **42**(4), 363–369. <https://doi.org/10.1081/clt-120039542>.
- Dwivedi, A. and Jain, M. K. (2014). Fly ash - waste management and overview: A Review. *Recent Research in Science and Technology*, **6**(1). <https://updatepublishing.com/journal/index.php/rrst/article/view/1157>
- Dzoujo, H. T., Shikuku, V. O., Tome, S., Akiri, S., Kengne, N. M., Abdpour, S., Janiak, C., Etoh, M. A., & Dina, D. (2022). Synthesis of pozzolan and sugarcane bagasse derived geopolymer-biochar composites for methylene blue sequestration from aqueous medium. *Journal of Environmental Management*, **318**(4), 115533. <https://doi.org/10.1016/j.jenvman.2022.115533>.
- El Alouani, M., Alehyen, S., El Achouri, M. and Taibi, M. (2018). Removal of Cationic Dye- Methylene Blue- from Aqueous Solution by Adsorption on Fly Ash-based geopolymer. *Journal of Materials and Environmental Science*, **9**(1), 32-46. <https://doi.org/10.26872/jmes.2018.9.1.5>.
- Ezemonye, L. and Tongo, I. (2010). Sublethal effects of endosulfan and diazinon pesticides on glutathione-S-transferase (GST) in various tissues of adult amphibians (*Bufo regularis*). *Chemosphere*, **81**(2), 214–217. <https://doi.org/10.1016/j.chemosphere.2010.06.039>.
- Fabricius, AL., Renner, M., Voss, M., Funk, M., Perfull, A., Gehring, F., Graf, R., Fromm, S., Duester, L. (2020). Municipal waste incineration fly ashes: from a multi-element approach to market potential evaluation. *Environmental Sciences Europe*, **32**, 88. <https://doi.org/10.1186/s12302-020-00365-y>.

- Freundlich, H.M.F., (1906). Über die adsorption in lösungen. *Zeitschrift für Physikalische Chemie*, **57**, 385–470.
- Fytianos, K., Voudrias, E., & Kokkalis, E. (2000). Sorption-desorption behaviour of 2,4-dichlorophenol by marine sediments. *Chemosphere*, **40**(1), 3–6.  
[https://doi.org/10.1016/S0045-6535\(99\)00214-3](https://doi.org/10.1016/S0045-6535(99)00214-3)
- Ghani, U., Hussain, S., ul-Amin, N., Imtiaz, M. and Khan, S.A. (2020). Laterite clay-based geopolymer as a potential adsorbent for the heavy metals removal from aqueous solutions. *Journal of Saudi Chemical Society*, **24**(11), 874-884.  
<https://doi.org/10.1016/j.jscs.2020.09.004>.
- Gupta, P., Nagpal, G. and Gupta, N. (2021). Fly ash based geopolymers: an emerging sustainable solution for heavy metal remediation from aqueous medium. *Beni-Suef University Journal of Basic and Applied Sciences*, **10**, 89.  
<https://doi.org/10.1186/s43088-021-00179-8>.
- Gupta, V.K., Imran, A. (2008). Removal of Endosulfan and Methoxychlor from Water on Carbon Slurry. *Environmental Science & Technology*, **42**(3), 766-770.  
<https://doi.org/10.1021/es7025032>.
- Hardjito, D., Wallah, S.E., Sumajouw, D.M., and Rangan, B.V. (2005). Fly Ash-Based Geopolymer Concrete. *Australian Journal of Structural Engineering*, **6**, 77 - 86.  
<https://doi.org/10.1080/13287982.2005.11464946>.
- Halsey, G. (1948). Physical adsorption on non-uniform surfaces. *Journal of Chemical Physics*, **16**, 931.  
<https://doi.org/10.1063/1.1746689>.
- Hengpraprom, S., Lee, C., Coates, J.T. (2006). Sorption of humic acids and alpha-endosulfan by clay minerals. *Environmental Toxicology and chemistry*, **25**(1), 11-7.  
<https://doi.org/10.1897/05-119r.1>.
- Hermann, D. T., Tome, S., Shikuku, V.O., Tchuigwa, J.T., Spieß, A., Janiak, C., Etoh, M.A., Dina, D. (2022). Enhanced Performance of Hydrogen Peroxide Modified Pozzolan-based Geopolymer for Abatement of Methylene blue from Aqueous Medium. *Silicon* **14**, 5191-5206. <https://doi.org/10.1007/s12633-021-01264-4>.
- Ho, Y.S and McKay, G. (1999). Pseudo-Second Order Model for Sorption Processes. *Process Biochemistry*, **34**(5), 451-465.  
[https://doi.org/10.1016/S0032-9592\(98\)00112-5](https://doi.org/10.1016/S0032-9592(98)00112-5).
- Hwang, J. I., Zimmerman, A. R. and Kim, J. E. (2018). Bioconcentration factor-based management of soil pesticide residues: Endosulfan uptake by carrot and potato plants. *The Science of the total environment*, **627**, 514–522.



<https://doi.org/10.1016/j.scitotenv.2018.01.208>.

- Ibrahim, W.M.W., Abdullah, M.M.A.B., Ahmad, R., Sandu, A.V., Vizureanu, P., Benjeddou, O., Rahim, A., Ibrahim, M., Sauffi, A.S. (2022). Chemical Distributions of Different Sodium Hydroxide Molarities on Fly Ash/Dolomite-Based Geopolymer. *Materials*, **15**, 6163. <https://doi.org/10.3390/ma15176163>
- lkowska, Z. D., Shyichuk, A., Karwasz, I., Witkowska, M., (2009). Adsorption of Cationic and Anionic Dyes onto Commercial Kaolin. *Adsorption Science & Technology*, **27**(2):205-214. <https://doi.org/10.1260/026361709789625306>.
- Innocenzi, P., Falcaro, P., Grosso, D. and Babonneau, F. (2003). Order-disorder transitions and evolution of silica structure in self- assembled mesostructured silica films studied through FTIR spectroscopy. *The Journal of Physical Chemistry B*, 2003, **107**(20), 4711-4717. <https://doi.org/10.1021/jp.026609z>.
- Irving, 1916 *J. Chem. Soc.*, 1940, 511-543. <https://doi.org/10.1039/JR9400000511>
- Jaarsveld, J., Van Deventer, J., and Lukey, G. (2002). The Effect of Composition and Temperature on Properties of Fly Ash and Kaolinite-Based Geopolymers. *Chemical Engineering Journal - CHEM ENG J.* **89**, 63-73. [https://doi.org/10.1016/S1385-8947\(02\)00025-6](https://doi.org/10.1016/S1385-8947(02)00025-6).
- Jemutai-Kimosop, S., Okello, V., Shikuku, V., Orata, F., Getenga, Z.M. (2022). Synthesis of mesoporous akaganeite functionalized maize cob biochar for adsorptive abatement of carbamazepine: Kinetics, isotherms, and thermodynamics. *Cleaner materials*, **5**, 100104. <https://doi.org/10.1016/j.clema.2022.100104>.
- Jia, H., Li, Y.F., Wang, D., Cai, D., Yang, M., Ma, J., Hu, J. (2009). Endosulfan in China 1-gridded usage inventories. *Environmental Science and Pollution Research*, **16**, 295–301. <https://doi.org/10.1007/s11356-008-0042-z>.
- Jiang, N., Shang, R., Heijman, S.G.J., & Rietveld, L.C. (2018). High-silica zeolites for adsorption of organic micro-pollutants in water treatment: A review. *Water Research*, **144**, 145-161.
- Karaer, H. and Kaya, I. (2016). Synthesis, characterization of magnetic chitosan/active charcoal composite and using at the adsorption of methylene blue and reactive blue. *Microporous and Mesoporous Materials*, **232**, 26-38. <https://doi.org/10.1016/j.micromeso.2016.06.006>.

- Kakoi, B., Kaluli, J.W., Thumbi, G. and Gachanja, A. (2015). Performance of activated carbon prepared from Sawdust as an adsorbent for endosulfan pesticide. *Journal of Sustainable Research in Engineering*, **2**(1), 1-10.
- Kataoka, R. and Takagi, K. (2013). Biodegradability and biodegradation pathways of endosulfan and endosulfan sulphate. *Applied Microbiology and Biotechnology*, **97**, 3285–3292. <https://doi.org/10.1007/s00253-013-4774-4>.
- Kawade, U.R., Hussain, M., and Shirule, P.A. (2016). Enhancement of compressive strength of geopolymer concrete by varying ratio of Na<sub>2</sub>SiO<sub>3</sub>/ NaOH and by varying molarity of NaOH. *International Journal of Latest Research in Engineering and Technology (IJLRET)*, **2**(8), 47-50. doi:10.4028/www.scientific.net/AMR.328-330.1475
- Kegley, S.E., Hill, B.R., Orme, S., Choi, A.H. (2010). Pesticide action network pesticide database. Pesticide action Network, North America, San Francisco CA.
- Kong, L., Zhu, S., Zhu, L., Xie, H., Su, K., Yan, T., Wang, J., Wang, J., Wang, F., Sun, F. (2010). Biodegradation of organochlorine pesticide endosulfan by bacterial strain *Alcaligenes faecalis* JBW4. *Journal of Environmental Sciences*, **25**(11), 2257-2264. [https://doi.org/10.1016/S1001-0742\(12\)60288-5](https://doi.org/10.1016/S1001-0742(12)60288-5).
- Kucuker, H., Sahin, O., Yavuz, Y., and Yürümez, Y. (2009). Fatal Acute Endosulfan Toxicity: A Case Report. *Basic and Clinical Pharmacology & Toxicology*, **104** (1), 49–51. <https://doi.org/10.1111/j.1742-7843.2008.00216.x>.
- Kughur, P.G. (2012). The effect of herbicides on crop production and environment in Makurdi local government area of Benue State, Nigeria. *Journal of Sustainable Development in Africa*, **14**(4), 1520-5509.
- Kumar, M., Lakshmi, C.V. and Khanna, S. (2008). Biodegradation and bioremediation of endosulfan contaminated soil. *Bioresource Technology*, **99** (8), 3116-3122. <https://doi.org/10.1016/j.biortech.2007.05.057>.
- Langmuir, I. (1918). The constitution and fundamental properties of solids and liquids, *Journal of the American Chemical Society*, **38**, 2221–2295.
- Li, K., Huang, G., Jiang, L., Cai, Y., Chen, J., and Ding, J. T. (2006). Study on Abilities of Mineral Admixtures and Geopolymer to Restrain ASR. *Key Engineering Materials - KEY ENG MAT.*, **302-303**. 248-254. <https://doi.org/10.4028/www.scientific.net/KEM.302-303.248>.
- Li, W., Dai, Y., Xue, B., Li, Y., Peng, X., Zhang, J., & Yan, Y. (2009). Biodegradation and detoxification of endosulfan in aqueous medium and soil by *Achromobacter*

- xylosoxidans strain CS5. *Journal of hazardous materials*, **167**(1-3), 209–216.  
<https://doi.org/10.1016/j.jhazmat.2008.12.111>
- Liu, Y., He, Z., Shankle, M., Tewolde, H. (2016). Compositional features of cotton plant biomass fractions characterized by attenuated total reflection Fourier transform infrared spectroscopy. *Industrial crops and products*, **79**, 283-286.
- Lubick N. (2010) Environment. Endosulfan's exit: U.S. EPA pesticide review leads to a ban. *Science*. **328** (5985), 1466.  
<https://doi.org/10.1126/science.328.5985.1466>.
- Luukkonen, T., Sarkkinen, M., Kempainen, K., Rämö, J., and Lassi, U. (2016). Metakaolin geopolymer characterization and application for ammonium removal from model solutions and landfill leachate. *Applied Clay Science*, **119** (2), 266-276.  
<https://doi.org/10.1016/j.clay.2015.10.027>.
- Mackenzie, K.J.D. and Welter, M. (2014). Geopolymer (aluminosilicate) composites: synthesis, properties and applications. *Advances in Ceramic Matrix Composites*, Woodhead Publishing, 445-470. <https://doi.org/10.1533/9780857098825.3.445>.
- Maingi, F.M., Mbuvi, H. M., Ng'ang'a, M.M. and Mwangi, H. (2017). Adsorption Kinetics and Isotherms of Methylene Blue by Geopolymers Derived from Common Clay and Rice Husk Ash. *Physical Chemistry*, **7**(4), 87-97.  
<http://doi:10.5923/j.pc.20170704.02>.
- Maleki, A., Hadizadeh, Z., Sharifi, V., Emdadi, Z. (2019). A green, porous and eco-friendly magnetic geopolymer adsorbent for heavy metals removal from aqueous solutions. *Journal of Cleaner Production*, **215**(1), 1233-1245.  
<https://doi.org/10.1016/j.jclepro.2019.01.084>
- Meroufel, B., Benali, O., Benyahia, M., Benmoussa, Y. and Zenasni, M.A. (2013). Adsorptive removal of anionic dye from aqueous solutions by Algerian kaolin: Characteristics, isotherm, kinetic and thermodynamic studies. *Journal of Materials and Environmental Science*, **4** (3), 482-491.
- Mishra, T. and Tiwari, S.K. (2006). Studies on sorption properties of zeolite derived from Indian fly ash. *Journal of hazardous materials*, **B137** (2006), 299-303.  
<https://doi.org/10.1016/j.jhazmat.2006.02.004>.
- Mi, J. and Jo, B. (2009). Acute endosulfan poisoning: a retrospective study. *Human and Experimental Toxicology*, **28**(5), 309-316.  
<https://doi.org/10.1177/0960327109106488>.

- Moses, V. and Peter, J. V. (2010). Acute intentional toxicity: endosulfan and other organochlorines. *Clinical toxicology (Philadelphia, Pa.)*, **48**(6), 539–544.  
<https://doi.org/10.3109/15563650.2010.494610>.
- Nath, P. and Sarker, P. (2017). Flexural strength and elastic modulus of ambient-cured blended low-calcium fly ash geopolymer concrete. *Construction and Building Materials*, **130**, 22-31. <http://doi.org/10.1016/j.conbuildmat.2016.11.034>.
- National Center for Biotechnology Information (2023). PubChem Compound Summary for CID 6434141. Retrieved February 14, 2023 from <https://pubchem.ncbi.nlm.nih.gov/compound/6434141>.
- Ofomaja, A. E. and Ho, Y. S. (2008). Effect of temperatures and pH on methyl violet biosorption by *Mansonia* wood sawdust. *Bioresource technology*, **99**(13), 5411–5417.  
<https://doi.org/10.1016/j.biortech.2007.11.018>.
- Owino, E. K., Shikuku, V. O., Nyairo, W. N., Kowenje, C. O., & Otieno, B. (2023). Valorization of solid waste incinerator fly ash by geopolymer production for removal of anionic bromocresol green dye from water: Kinetics, isotherms and thermodynamics studies. *Sustainable Chemistry for the Environment*, **3**, 100026.  
<https://doi.org/10.1016/j.scenv.2023.100026>
- Parbhu, B., Rodgers, G., and Sullivan, J.E. (2009). Death in a toddler following endosulfan ingestion. *Clinical Toxicology*, **47**(9), 899-901.  
<https://doi.org/10.3109/15563650903328879>.
- Patankar, S.V., Ghugal, Y.M., Jamkar, S.S. (2015). Mix Design of Fly Ash Based Geopolymer Concrete. In: *Matsagar, V. (eds) Advances in Structural Engineering. Springer, New Delhi*. [https://doi.org/10.1007/978-81-322-2187-6\\_123](https://doi.org/10.1007/978-81-322-2187-6_123).
- Patocka J., Wu Q., Franca T.C.C., Ramalho, T.C., Pita R. and Kuca, K. (2016). Clinical aspects of the poisoning by the pesticide endosulfan. *Química Nova*, **39**(8), 987-994.  
<http://dx.doi.org/10.5935/0100-4042.20160102>.
- Pereira, R.C., Anizelli, P.R., Di Mauro, E., Valezi, D.F., da Costa, A.C.S., Zaia, C.T.B.V., Zaia, D.A.M.(2019). The effect of pH and ionic strength on the adsorption of glyphosate onto ferrihydrite. *Geochemical Transactions*, **20** (3).  
<https://doi.org/10.1186/s12932-019-0063-1>.
- Peydayesh, M., Isanejad, M., Mohammadi, T., Jafari, S.M.R.S. (2015). Assessment of *Urtica* as a low-cost adsorbent for methylene blue removal: kinetic, equilibrium, and thermodynamic studies. *Chemical Papers- Slovak Academy of Sciences*, **69**, 930–937. <https://doi.org/10.1515/chempap-2015-0097>.

- Phair, J.W., and Van Deventer, J.S.J., (2001). Effect of silicate activator pH on the leaching and material characteristics of waste-based inorganic polymers. *Minerals Engineering*, **14**(3), 289-304. [https://doi.org/10.1016/S0892-6875\(01\)00002-4](https://doi.org/10.1016/S0892-6875(01)00002-4).
- Polati, S., Angioi, S., Gianotti, V., Gosetti, F. and Genarro, M.C. (2006). Sorption of pesticides on Kaolinite and Montmorillonite as a function of hydrophilicity. *Journal of Environmental Science and Health*, part B, **41**(4), 333-344. <https://doi.org/10.1080/03601230600591416>.
- Provis, J. and Van Deventer, J. (2007). Geopolymerisation kinetics. 2. Reaction kinetic modelling. *Chemical Engineering Science*. **62**, 2318-2329. <https://doi.org/10.1016/j.ces.2007.01.028>.
- Qiu, L., Jia, K., Huang, L., Liao, X., Guo, X., Lu, H. (2019) Hepatotoxicity of tricyclazole in zebrafish (*Danio rerio*). *Chemosphere*, **232**, 171-179.
- Ramaswamy, J. and Vasudevan, N. (2008). Bioremediation of pesticide (endosulfan) contaminated soils. *Asian Journal of Microbiology, Biotechnology and Environmental Sciences*, **10**, 527-532.
- Rashed, M. N., (2013). Adsorption Technique for the Removal of Organic Pollutants from Water and Wastewater. *Organic Pollutants - Monitoring, Risk and Treatment*. <https://doi.org/10.5772/54048>.
- Rauf, N., Tahir, S.S., Kang, J.H. and Chang, Y.S. (2012). Equilibrium, thermodynamics and kinetics studies for the removal of alpha and beta endosulfan by adsorption onto bentonite clay. *Chemical Engineering Journal*, **192**, 369-376. <https://doi.org/10.1016/j.cej.2012.03.047>.
- Revellame, E. D., Fortela, D. L., Sharp, W., Hernandez, R. and Zappi, M. E. (2020). Adsorption kinetic modelling using pseudo-first order and pseudo-second order rate laws: A review. *Cleaner Engineering and Technology*, 1. <https://doi.org/10.1016/j.clet.2020.100032>.
- Roberts, E.M., English, P.B., Grether, J.K., Windham, G.C., Somberg, L. and Wolff, C. (2007). Maternal residence near agricultural pesticide applications and autism spectrum disorders among children in the California Central Valley. *Environmental Health Prospects*, **115**(10). <https://doi.org/10.1289/ehp.10168>.

- Sarkar, C., Basu, J.K. and Samanta, A.N. (2017). Removal of Ni<sup>2+</sup> ion from waste water by geopolymeric adsorbent derived from LD slag. *Journal of Water Process Engineering*, **17**, 237-244. <https://doi.org/10.1016/j.jwpe.2017.04.012>.
- Sarkar, C., Basu, J.K., Samanta, A.N. (2019). Experimental and kinetic study of fluoride adsorption by Ni and Zn modified LD slag based geopolymer. *Chemical Engineering Research and Design*, **142**, 165-175. <https://doi.org/10.1016/j.cherd.2018.12.006>.
- Sammaiah, D., Shekar, C., Prasad, V. and Jaganmohan, K. (2011). Pesticides induced alterations in physiological responses in Solanum melongena L. *International Journal of Pharma and Bio Sciences*, **2**, 374-384.
- Satar, S., Sebe, A., Alpaya, N. R., Gumusay, U., & Guneyssel, O. (2009). Unintentional endosulfan poisoning. *Bratislavské lekárske listy*, **110**(5), 301–303.
- Shikuku, V.O. and Kimosop, S. (2020). Efficient removal of sulfamethoxazole onto sugarcane bagasse-derived biochar: Two and Three-parameter isotherms, kinetics, thermodynamics. *South African Journal of Chemistry*, **73**, 111-118. <http://dx.doi.org/10.17159/0379-4350/2020/v73a16>.
- Shikuku, V.O., Kowenje, C.O., Kengara, F. (2018). Errors in Parameters Estimation using Linearized Adsorption Isotherms: Sulfadimethoxine Adsorption onto Kaolinite Clay. *Chem. Sci. Inter. J.* **23**, 1-6.
- Shikuku, V. O. & Sylvain, T. (2019). Application of Geopolymer Composites in Wastewater Treatment: Trends, Opportunities, and Challenges. In N. Ramdani (Ed.), *Polymer Nanocomposites for Advanced Engineering and Military Applications*, pp. 131-149. IGI Global. <https://doi.org/10.4018/978-1-5225-7838-3.ch005>.
- Shikuku, V.O. and Tome, S., Dzoujo, T.H., Thompsett, G.A. and Timko, M.T. (2022). Rapid Adsorption of Cationic Methylene Blue dye onto volcanic ash-metakaolin based geopolymers. *Silicon*, **14**, 9349-9359. <https://doi.org/101007/s12633-021-01637-9>.
- Shikuku, V.O., Zanella, R., Kowenje, C.O., Donato, F.F., Bandeira, N.M.G. and Prestes, O.D. (2018). Single and binary adsorption of sulfonamide antibiotics onto iron-modified clay: linear and nonlinear isotherms, kinetics, thermodynamics, and mechanistic studies. *Applied Water Science*, **8**, 175. <https://doi.org/10.1007/s13201-018-0825-4>.
- Shivaramaiah, H. M., & Kennedy, I. R. (2006). Biodegradation of endosulfan by a soil bacterium. *Journal of environmental science and health. Part. B, Pesticides, food contaminants, and agricultural wastes*, **41**(6), 895–905.

<https://doi.org/10.1080/03601230600806004>.

- Shokrollahi, A., Alizadeh, A., Malekhosseini, Z. and Ranjbar, M. (2011). Removal of Bromocresol Green from Aqueous Solution via Adsorption on Ziziphus Nummularia as a New, Natural, and Low-Cost Adsorbent: Kinetic and Thermodynamic Study of Removal Process. *Journal of Chemical and Engineering Data*, **15**, 3738–3746. <https://doi.org/10.1021/je200311y>.
- Sipes, N. S., Martin, M. T., Kothiya, P., Reif, D. M., Judson, R. S., Richard, A. M., Houck, K. A., Dix, D. J., Kavlock, R. J., & Knudsen, T. B. (2013). Profiling 976 Toxicant chemicals across 331 enzymatic and receptor signalling assays. *Chemical research in toxicology*, **26**(6), 878–895. <https://doi.org/10.1021/tx400021f>.
- Siyal, A. A., Shamsuddin, M. R., Khan, M. I., Rabat, N.E., Zulfiqar, M., Man, Z., Low A. (2019). Fly ash based geopolymer for the adsorption of anionic surfactant from aqueous solution. *Journal of Cleaner Production*, **229**, 232-243. <https://doi.org/10.1016/j.jclepro.2019.04.384>.
- Siyal, A. A., Shamsuddin, M. R., Khan, M. I., Rabat, N.E., Zulfiqar, M., Man, Z., Siame, J., Azizli, K.A. (2018). A review on geopolymers as emerging materials for the adsorption of heavy metals and dyes. *J. Environ. Manag.* **224**, 327-339. <https://doi.org/10.1016/j.jenvman.2018.07.046>.
- Siyal, A.A., Azizli, K.A., Man, Z., Ullah, H., (2016). Effects of parameters on the setting time of fly ash based geopolymers using Taguchi method. *Procedia Engineering*, **148**, 302-307. <http://creativecommons.org/licenses/by-nc-nd/4.0/>.
- Sudhakar Y. & Dikshit A. K. (1999). Adsorbent selection for endosulfan removal from water environment. *Journal of Environmental Science and Health, Part B*, **34**:1, 97-118, <https://doi.org/10.1080/03601239909373186>
- Sumajouw, M.D.J. and Rangan, B.V., 2006. Low-Calcium fly ash-based geopolymer concrete: Reinforced beams and columns. Curtin University of Technology. <http://hdl.handle.net/20.500.11937/23928>.
- Swanepoel, J.C. and Strydom, C.A. (2002). Utilisation of fly ash in a geopolymeric material. *Applied Geochemistry*, **17**(8), 1143-1148. [https://doi.org/10.1016/S0883-2927\(02\)00005-7](https://doi.org/10.1016/S0883-2927(02)00005-7).
- Thangadurai, P. and Suresh, S. (2014). Biodegradation of endosulfan by soil bacterial cultures. *International Biodeterioration & Biodegradation*, **94**, 38-47. <https://doi.org/10.1016/j.ibiod.2014.06.017>.

- Tome, S., Etoh, M.-A., Etame, J., Sanjay, K. (2018). Characterization and Leachability Behaviour of Geopolymer Cement Synthesised from Municipal Solid Waste Incinerator Fly Ash and Volcanic Ash Blends. *Recycling*, **3**(4), 50. <https://doi.org/10.3390/recycling3040050>.
- Tome, S., Dzoujo, T.H., Shikuku, V.O., Otieno, S. (2021). Synthesis, characterization and application of acid and alkaline activated volcanic ash-based geopolymers for adsorptive remotion of cationic and anionic dyes from water. *Ceramics International*, **47** (15), 20965-20973. <https://doi.org/10.1016/j.ceramint.2021.04.097>.
- Tome, S., Shikuku, V., Tamaguelon, H.D. *et al.* (2023). Efficient sequestration of malachite green in aqueous solution by laterite-rice husk ash-based alkali-activated materials: parameters and mechanism. *Environ Sci Pollut Res* **30**, 67263–67277. <https://doi.org/10.1007/s11356-023-27138-3>
- Treybal, R.E. (1980). Mass Transfer Operations, 3rd edn. McGraw-Hill, New York, USA.
- Van Deventer, J.S.J., Provis, J.L., Duxson, P., Lukey, G.C. (2007). Reaction mechanisms in the geopolymeric conversion of inorganic waste to useful products. *Journal of Hazardous Materials*. **139** (3), 506-513. <https://doi.org/10.1016/j.jhazmat.2006.02.044>.
- Verma, A., Ali, D., Farooq, M., Pant, A.B., Ray, R.S., Hans, R.K. (2011). Expression and inducibility of endosulfan metabolizing gene in *Rhodococcus* strain isolated from earthworm gut microflora for its application in bioremediation. *Bioresource Technology*, **102**(3), 2979-2984. <https://doi.org/10.1016/j.biortech.2010.10.005>.
- Wan, M.T., Kuo, J. and Pasternak, J. (2005). Residues of Endosulfan and Other Selected Organochlorine Pesticides in Farm Areas of the Lower Fraser Valley, British Columbia, Canada. *Journal of Environmental Quality*, **34**(4), 1186-1193. <https://doi.org/10.2134/jeq2004.0361>.
- Weber, J., Halsall, C. J., Muir, D., Teixeira, C., Small, J., Solomon, K., Hermanson, M., Hung, H., & Bidleman, T. (2010). Endosulfan, a global pesticide: a review of its fate in the environment and occurrence in the Arctic. *The Science of the total environment*, **408**(15), 2966–2984. <https://doi.org/10.1016/j.scitotenv.2009.10.077>.
- Weber, T.W. and Chakravo, R.K. (1974) Pore and Solid Diffusion Models for Fixed-Bed Adsorbers. *AIChE Journal*, **20**, 228-238. <http://dx.doi.org/10.1002/aic.690200204>.
- Xinghua, H., Shujing, Z. and Hwang, J.Y. (2016). Physical and Chemical Properties of MSWI Fly ash. In: Ikhmayies, S.J., *et al.* *Characterization of Minerals, Metals, and Materials 2016*. Springer, Cham. [https://doi.org/10.1007/978-3-319-48210-1\\_56](https://doi.org/10.1007/978-3-319-48210-1_56)



- Xu, H. and Van Deventer, J. (2002). Geopolymerisation of Multiple Minerals. *Minerals Engineering - MINER ENG.* **15**, 1131-1139.  
[https://doi.org/10.1016/S0892-6875\(02\)00255-8](https://doi.org/10.1016/S0892-6875(02)00255-8).
- Xu, H., Van Deventer, J. and Lukey, G. (2001). Effect of Alkali Metals on the Preferential Geopolymerization of Stilbite/Kaolinite Mixtures. *Industrial & Engineering Chemistry Research-IND ENG CHEM RES.* **40**, **17**, 3749-3756.  
<https://doi.org/10.1021/ie010042b>
- Yedla, S. and Dikshit, A. (2008). Removal of Endosulfan from Water Using Wood Charcoal-Adsorption and Desorption. *Journal of Environmental Engineering-asce - J ENVIRON ENG-ASCE.*, **134**(2).  
[http://dx.doi.org/10.1061/\(ASCE\)0733-9372\(2008\)134:2\(102\)](http://dx.doi.org/10.1061/(ASCE)0733-9372(2008)134:2(102)).
- Yonli, A. H., Batonneau-Gener, I. and Koulidiati, J. (2012). Adsorptive removal of  $\alpha$ -endosulfan from water by hydrophobic zeolites. An isothermal study. *Journal of hazardous materials*, **203-204**, 357–362.  
<https://doi.org/10.1016/j.jhazmat.2011.12.042>.
- Yuh-Shan, H. (2004). Citation Review of Lagergren Kinetic Rate Equation on Adsorption Reactions. *Scientometrics*, **59** (1), 171-177.  
<https://doi.org/10.1023/B:SCIE.0000013305.99473.cf>.
- Zhang, Z., Yao, X. and Wang, H., (2012). Potential application of geopolymers as protection coatings for marine concrete III. Field experiment. *Applied Clay Science*, **67-68**, 57-60. <https://doi.org/10.1016/j.clay.2012.05.008>.
- Zulkifly, K., Yong, H.C., Abdullah, M.M.B., Ming, L.Y., Sandu, A.V. and Abdullah, S.F.A. (2019). Characterization of Fly Ash and Metakaolin Blend Geopolymers under Ambient Temperature Condition. *Materials Science and Engineering* **551**, 012086.  
<https://doi.org/10.1088/1757-899X/551/1/012086>.

## APPENDICES

### *Appendix 1: Statistical analysis of the kinetic data using originPro 9.0 software*

ANOVAOneWay (20/11/2023 08:41:47)

#### *Descriptive Statistics*

	N Analysis	N Missing	Mean	Standard Deviation	SE of Mean
GPA	1	0	2.00564	--	--
GPB	9	0	4.9772	1.72797	0.57599
GPC	9	0	5.15652	1.73298	0.57766
MWFA	9	0	1.67262	0.73235	0.24412

#### *One Way ANOVA*

##### *Overall ANOVA*

	DF	Sum of Squares	Mean Square	F Value	Prob>F
Model	3	72.8612	24.28707	11.16571	8.83569E-5
Error	24	52.20354	2.17515		
Total	27	125.06474			

Null Hypothesis: The means of all levels are equal.

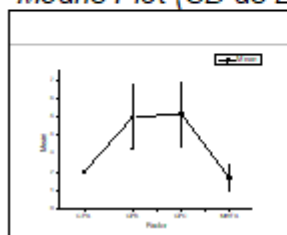
Alternative Hypothesis: The means of one or more levels are different.

At the 0.05 level, the population means are significantly different.

#### *Fit Statistics*

	R-Square	Coeff Var	Root MSE	Data Mean
	0.58259	0.38144	1.47484	3.86652

#### *Means Plot (SD as Error)*



*Appendix 2: Statistical analysis of the thermodynamic data using originPro 9.0 software*

ANOVAOneWay (20/11/2023 08:13:43)

*Descriptive Statistics*

	N Analysis	N Missing	Mean	Standard Deviation	SE of Mean
GPA	1	0	6.38613	--	--
GPB	6	0	7.02015	0.61756	0.25212
GPC	6	0	7.13543	0.58212	0.23765
MWFA	6	0	1.98642	0.42146	0.17206

*One Way ANOVA*

*Overall ANOVA*

	DF	Sum of Squares	Mean Square	F Value	Prob>F
Model	3	104.68563	34.89521	116.59375	1.28291E-10
Error	15	4.48933	0.29929		
Total	18	109.17497			

Null Hypothesis: The means of all levels are equal.

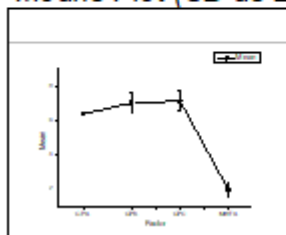
Alternative Hypothesis: The means of one or more levels are different.

At the 0.05 level, the population means are significantly different.

*Fit Statistics*

	R-Square	Coeff Var	Root MSE	Data Mean
	0.95888	0.10068	0.54707	5.43359

*Means Plot (SD as Error)*



**Appendix 3: Statistical analysis of the Langmuir adsorption isotherm data using originPro 9.0 software**

ANOVAOneWay (20/11/2023 08:28:44)

**Descriptive Statistics**

	N Analysis	N Missing	Mean	Standard Deviation	SE of Mean
GPA	1	0	3.42362	--	--
GPB	5	0	10.01725	5.08023	2.27195
GPC	5	0	10.06336	5.16808	2.31124
MWFA	5	0	1.48681	0.56431	0.25237

**One Way ANOVA**

**Overall ANOVA**

	DF	Sum of Squares	Mean Square	F Value	Prob>F
Model	3	257.17248	85.72416	4.86735	0.01933
Error	12	211.34508	17.61209		
Total	15	468.51756			

Null Hypothesis: The means of all levels are equal.

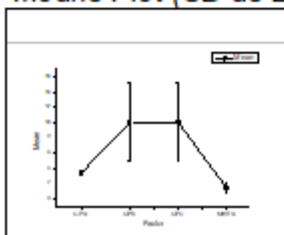
Alternative Hypothesis: The means of one or more levels are different.

At the 0.05 level, the population means are significantly different.

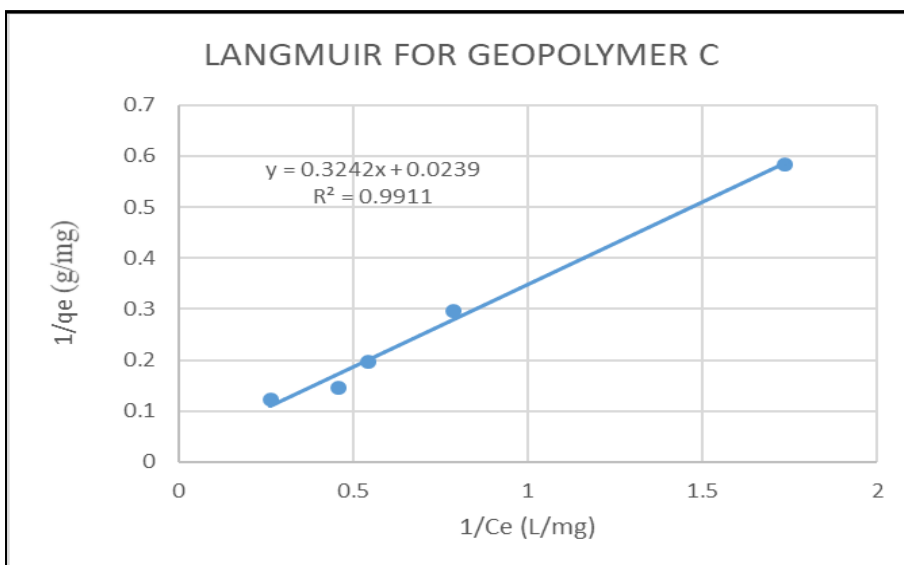
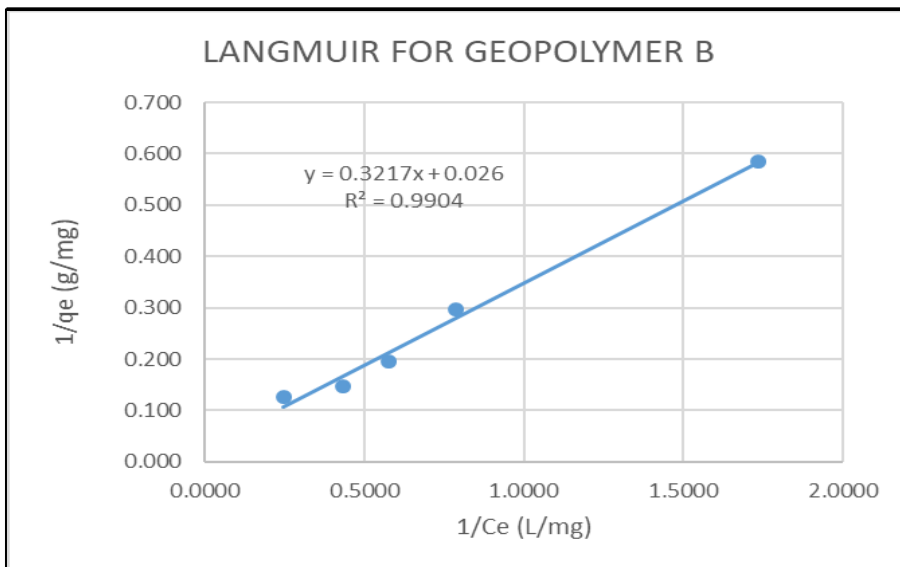
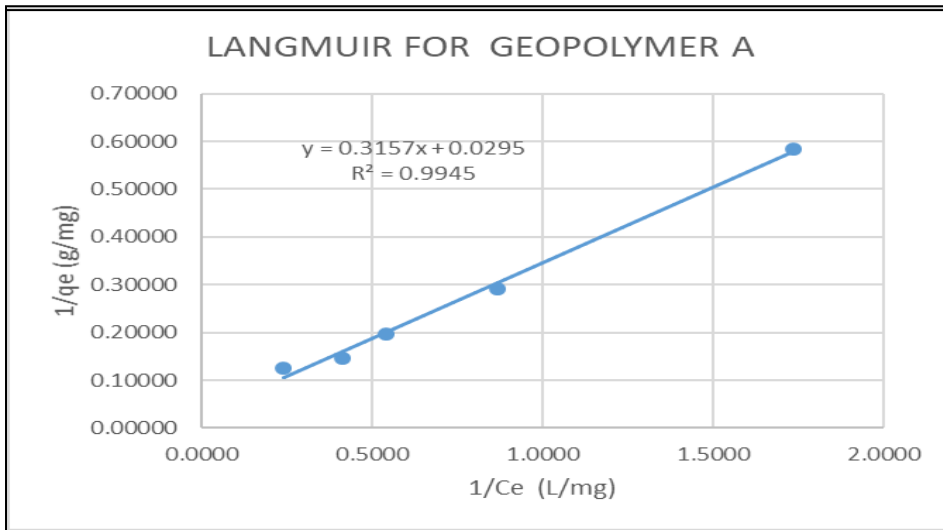
**Fit Statistics**

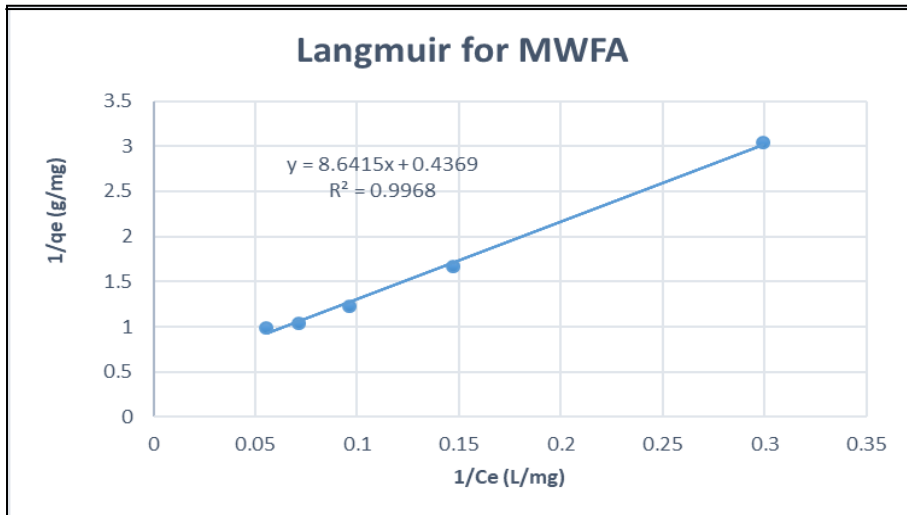
	R-Square	Coeff Var	Root MSE	Data Mean
	0.54891	0.60351	4.19668	6.95379

**Means Plot (SD as Error)**

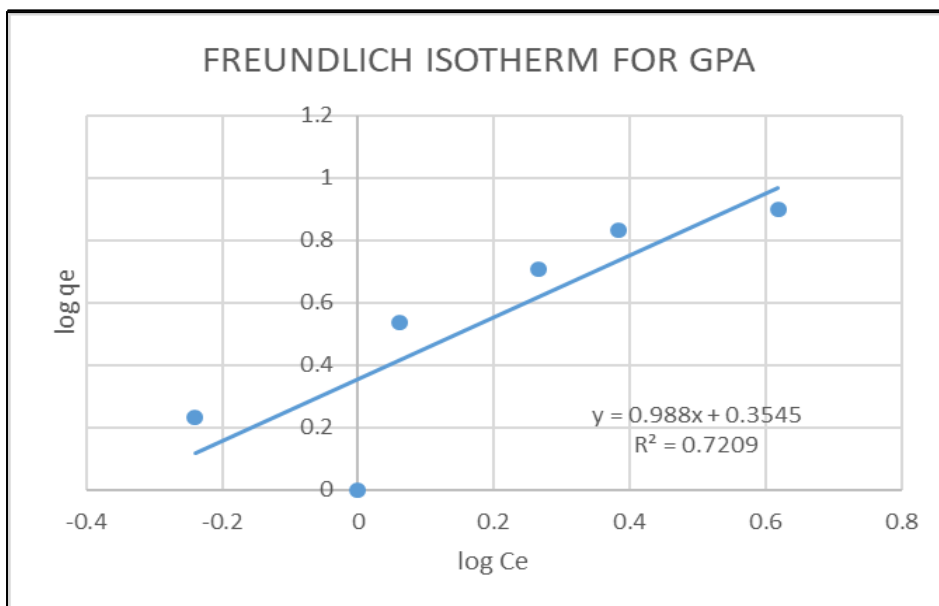


**Appendix 4: Langmuir adsorption isotherm using excel**

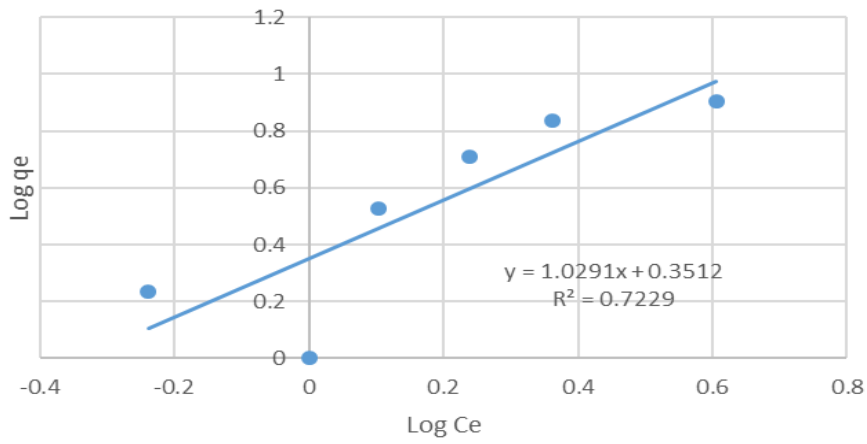




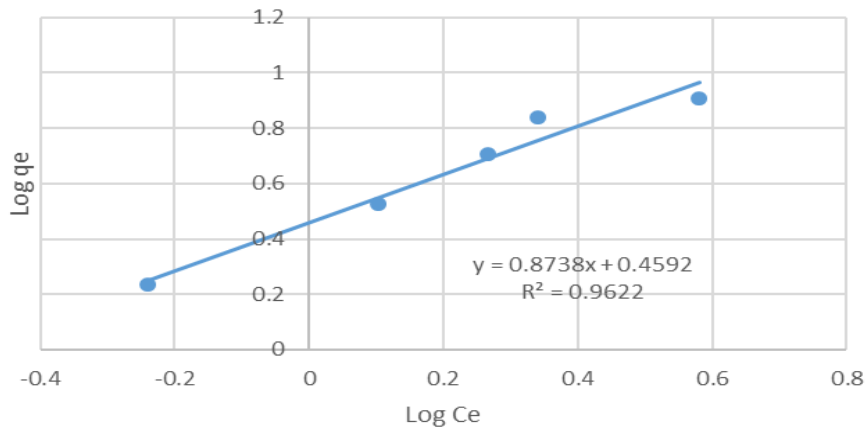
*Appendix 5: Freundlich adsorption isotherm using excel*



FREUNDLICH ISOTHERM FOR GPB



FREUNDLICH ISOTHERM FOR GPC



FREUNDLICH ISOTHERM FOR MWFA

